particles

IMPACT FACTOR 1.7

CITESCORE 3.2

Review

On the Energy Budget of Quarks and Hadrons, Their Inconspicuous "Strong Charge", and the Impact of Coulomb Repulsion on the Charged Ground States

Dimitris M. Christodoulou and Demosthenes Kazanas

MDPI

https://doi.org/10.3390/particles7030038

particles

MDPI

Review

On the Energy Budget of Quarks and Hadrons, Their Inconspicuous "Strong Charge", and the Impact of Coulomb Repulsion on the Charged Ground States

Dimitris M. Christodoulou [1,*,†] and Demosthenes Kazanas [2,†]

[1] Lowell Center for Space Science and Technology, University of Massachusetts Lowell, Lowell, MA 01854, USA
[2] NASA/GSFC, Astrophysics Science Division, Code 663, Greenbelt, MD 20771, USA; demos.kazanas@nasa.org
* Correspondence: dimitris_christodoulou@uml.edu
† The authors contributed equally to this work.

Abstract: We review and meta-analyze particle data and properties of hadrons with measured rest masses. The results of our study are summarized as follows. (1) The strong-force suppression of the repulsive Coulomb forces between quarks is sufficient to explain the differences between mass deficits in nucleons and pions (and only them), the ground states with the longest known mean lifetimes; (2) unlike mass deficits, the excitations in rest masses of all particle groups are effectively quantized, but the rules are different in baryons and mesons; (3) the strong field is aware of the extra factor of $\vartheta_e = 2$ in the charges (Q) of the positively charged quarks; (4) mass deficits incorporate contributions proportional to the mass of each valence quark; (5) the scaling factor of these contributions is the same for each quark in each group of particles, provided that the factor $\vartheta_e = 2$ is taken into account; (6) besides hypercharge (Y), the much lesser-known "strong charge" ($Q' = Y - Q$) is very useful in SU(3) in describing properties of particles located along the right-leaning sides and diagonals of the weight diagrams; (7) strong decays in which Q' is conserved are differentiated from weak decays, even for the same particle; and (8) the energy diagrams of (anti)quark transitions indicate the origin of CP violation.

Keywords: CP violation; flavor symmetries; properties of hadrons; quark masses; quark–gluon plasma

MSC: 81-10; 81R40; 81U90; 81V05; 81V10

Citation: Christodoulou, D.M.; Kazanas, D. On the Energy Budget of Quarks and Hadrons, Their Inconspicuous "Strong Charge", and the Impact of Coulomb Repulsion on the Charged Ground States. *Particles* **2024**, *7*, 653–682. https://doi.org/10.3390/particles7030038

Academic Editor: Armen Sedrakian

Received: 6 June 2024
Revised: 17 July 2024
Accepted: 24 July 2024
Published: 26 July 2024

1. Introduction

Herein, we revisit the experimental results and the quantum properties relating to hadrons with measured rest masses. Our data come from the extensive work of the Particle Data Group (PDG) and from CODATA constants [1–3]. In this work, we focus on the mass deficits of particles [4] and on the SU(3) quantum numbers that describe symmetries of the strong force. All revisited physical quantities and SU(3)/SU(2) numbers are defined in Table 1 before they are listed in subsequent tables and used in the text. Our compilations of properties and derived quantum numbers are then shown in Tables 2–4 for baryons with spin parities ($J^P = (1/2)^+$ and $J^P = (3/2)^+$), as well as for pseudo-scalar mesons with $J^P = 0^-$ and vector mesons with $J^P = 1^-$. Following standard convention, masses and mass deficits are listed in units of energy (MeV), and electromagnetic (EM) charges (Q) are listed in units of the elementary charge ($e = 1.6022 \times 10^{-19}$ Cb, where Cb stands for the SI unit of Coulomb [3]).

Table 1. Definitions of physical quantities and quantum numbers considered in this review.

Quantity/Number	Symbol	Definition for a Particle
$\text{Spin}^{\text{Parity}}$	J^{P}	Intrinsic angular $\text{momentum}^{\text{Reflection symmetry}}$
Rest mass	M	Invariant mass–energy content
Mass deficit	MD	$= M -$ (valence (anti)quark masses); also called "mass defect" [4]
Binding factor	BF	$= MD$ divided by a linear combination of valence (anti)quark masses; see, e.g., Equations (2) and (3) in the text
Strangeness	S	$= -(n_{\text{s}} - n_{\bar{\text{s}}})$ for s quarks and $\bar{\text{s}}$ antiquarks
Charm	C	$= +(n_{\text{c}} - n_{\bar{\text{c}}})$ for c quarks and $\bar{\text{c}}$ antiquarks
Bottomness	B'	$= -(n_{\text{b}} - n_{\bar{\text{b}}})$ for b quarks and $\bar{\text{b}}$ antiquarks
Total isospin	I	A subset of flavor symmetry for u and d quarks and their antiquarks
Isospin component 3	I_3	Component 3 of isospin vector $I = (I_1, I_2, I_3)$
Hypercharge	Y	$= \mathcal{B} + S - (C - B' + T')/3$, where $\mathcal{B}$ is the baryon number and the topness is $T' = 0$ for all known particles [2]
Electric charge	Q	The physical property of the electromagnetic field
"Strong charge"	Q'	$= Y - Q$; see, e.g., Equation (13) in the text
Weak isospin component 3	$I_{3\text{w}}$	Component 3 of weak isospin vector I_{w} (SU(2) only)
Weak hypercharge	Y_{w}	$= 2(Q - I_{3\text{w}})$
"Weak charge"	Q'_{w}	$= Y_{\text{w}} - Q$

Table 2. The $J^{\text{P}} = (1/2)^+$ baryon octet followed by additional high-mass $J^{\text{P}} = (1/2)^+$ baryon states $^{(\star)}$.

Particle Symbol	Quark Content	Rest Mass M (MeV)	Q (e)	I	S	C	B'	I_3	Y	Q'	BF	MD (MeV)
p^+	uud	938.27208	+1	1/2	0	0	0	1/2	1	0	69.8	929.2821
n^0	udd	939.56541	0	1/2	0	0	0	−1/2	1	1	67.9	928.0654
Λ^0	uds	1115.683	0	0	−1	0	0	0	0	0	9.92	1015.45
Σ^0	uds	1192.642	0	1	−1	0	0	0	0	0	10.7	1092.41
Σ^+	uus	1189.37	+1	1	−1	0	0	1	0	−1	10.7	1091.65
Σ^-	dds	1197.449	−1	1	−1	0	0	−1	0	1	10.7	1094.71
Ξ^0	uss	1314.86	0	1/2	−2	0	0	1/2	−1	−1	5.89	1125.90
Ξ^-	dss	1321.71	−1	1/2	−2	0	0	−1/2	−1	0	5.90	1130.24
Λ_{c}^+	udc	2286.46	+1	0	0	1	0	0	2	1	0.396	1009.6
Λ_{b}^0	udb	5619.6	0	0	0	0	−1	0	0	0	0.342	1432.8
Σ_{c}^{++}	uuc	2453.97	+2	1	0	1	0	1	2	0	0.463	1179.6
Σ_{c}^+	udc	2452.9	+1	1	0	1	0	0	2	1	0.461	1176.1
Σ_{c}^0	ddc	2453.75	0	1	0	1	0	−1	2	2	0.461	1174.4
$\Xi_{\text{c}}'^+$	usc	2578.4	+1	1/2	−1	1	0	1/2	1	0	0.460	1212.8
$\Xi_{\text{c}}'^0$	dsc	2579.2	0	1/2	−1	1	0	−1/2	1	1	0.459	1211.1
Ω_{c}^0	ssc	2695.2	0	0	−2	1	0	0	0	0	0.454	1238.4
Σ_{b}^+	uub	5810.56	+1	1	0	0	−1	1	0	−1	0.388	1626.2
Σ_{b}^0	udb	(5810.56)	0	1	0	0	−1	0	0	0	0.388	1623.7
Σ_{b}^-	ddb	5815.64	−1	1	0	0	−1	−1	0	1	0.388	1626.3
Ω_{b}^-	ssb	6046.1	−1	0	−2	0	−1	0	−2	−1	0.385	1679.3
Ξ_{c}^+	usc	2467.94	+1	1/2	−1	1	0	1/2	1	0	0.418	1102.4
Ξ_{c}^0	dsc	2470.90	0	1/2	−1	1	0	−1/2	1	1	0.418	1102.8
Ξ_{cc}^{++}	ucc	3621.2	+2	1/2	0	2	0	1/2	3	1	0.212	1079.0
Ξ_{cc}^+	dcc	(3621.2)	+1	1/2	0	2	0	−1/2	3	2	0.212	1076.5
Ξ_{b}^0	usb	5791.9	0	1/2	−1	0	−1	1/2	−1	−1	0.354	1516.3
Ξ_{b}^-	dsb	5797.0	−1	1/2	−1	0	−1	−1/2	−1	0	0.355	1518.9
$\Xi_{\text{b}}'^0$	usb	(5791.9)	0	1/2	−1	0	−1	1/2	−1	−1	0.354	1516.3
$\Xi_{\text{b}}'^-$	dsb	(5797.0)	−1	1/2	−1	0	−1	−1/2	−1	0	0.355	1518.9

$^{(\star)}$ All listed quantities are defined in Table 1.

Table 3. The $J^P = (3/2)^+$ baryon decuplet followed by an additional $J^P = (3/2)^+$ baryon states [⋆].

Particle Symbol	Quark Content	Rest Mass M (MeV)	Q (e)	I	S	C	B'	I_3	Y	Q'	BF	MD (MeV)
Δ^{++}	uuu	1232	+2	3/2	0	0	0	3/2	1	−1	94.6	1225.5
Δ^{+}	uud	1232	+1	3/2	0	0	0	1/2	1	0	91.9	1223.0
Δ^{0}	udd	1232	0	3/2	0	0	0	−1/2	1	1	89.3	1220.5
Δ^{-}	ddd	1232	−1	3/2	0	0	0	−3/2	1	2	86.9	1218.0
Σ^{*+}	uus	1382.80	+1	1	−1	0	0	1	0	−1	12.6	1285.1
Σ^{*0}	uds	1383.7	0	1	−1	0	0	0	0	0	12.5	1283.5
Σ^{*-}	dds	1387.2	−1	1	−1	0	0	−1	0	1	12.5	1284.5
Ξ^{*0}	uss	1531.80	0	1/2	−2	0	0	1/2	−1	−1	7.03	1342.8
Ξ^{*-}	dss	1535.0	−1	1/2	−2	0	0	−1/2	−1	0	7.02	1343.5
Ω^{-}	sss	1672.45	−1	0	−3	0	0	0	−2	−1	4.97	1392.3
Σ_c^{*++}	uuc	2518.41	+2	1	0	1	0	1	2	0	0.488	1244.1
Σ_c^{*+}	udc	2517.5	+1	1	0	1	0	0	2	1	0.487	1240.7
Σ_c^{*0}	ddc	2518.48	0	1	0	1	0	−1	2	2	0.486	1239.1
Ξ_c^{*+}	usc	2645.56	+1	1/2	−1	1	0	1/2	1	0	0.485	1280.0
Ξ_c^{*0}	dsc	2646.38	0	1/2	−1	1	0	−1/2	1	1	0.485	1278.3
Ω_c^{*0}	ssc	2765.9	0	0	−2	1	0	0	0	0	0.480	1309.1
Σ_b^{*+}	uub	5830.32	+1	1	0	0	−1	1	0	−1	0.393	1646.0
Σ_b^{*0}	udb	(5830.32)	0	1	0	0	−1	0	0	0	0.392	1643.5
Σ_b^{*-}	ddb	5834.74	−1	1	0	0	−1	−1	0	1	0.393	1645.4
Ξ_b^{*0}	usb	5952.3	0	1/2	−1	0	−1	1/2	−1	−1	0.392	1676.7
Ξ_b^{*-}	dsb	5955.33	−1	1/2	−1	0	−1	−1/2	−1	0	0.392	1677.3

[⋆] All listed quantities are defined in Table 1.

Table 4. The $J^P = 0^-$ pseudoscalar meson nonet followed by additional meson states (the $J^P = 0^-$ high-mass η mesons, D mesons, and B mesons and the $J^P = 1^-$ vector mesons) [⋆].

Particle Symbol	Quark Content	Rest Mass M (MeV)	Q (e)	I	S	C	B'	I_3	Y	Q'	BF	MD (MeV)
π^{+}	$u\bar{d}$	139.5704	+1	1	0	0	0	1	0	−1	14.8	132.74
π^{-}	$d\bar{u}$	139.5704	−1	1	0	0	0	−1	0	1	14.8	132.74
π^{0}	$\frac{u\bar{u}-d\bar{d}}{\sqrt{2}}$	134.9768	0	1	0	0	0	0	0	0	14.3	128.15
η	$\frac{u\bar{u}+d\bar{d}-2s\bar{s}}{\sqrt{6}}$	547.862	0	0	0	0	0	0	0	0	...	...
η'	$\frac{u\bar{u}+d\bar{d}+s\bar{s}}{\sqrt{3}}$	957.78	0	0	0	0	0	0	0	0	...	...
K^{+}	$u\bar{s}$	493.677	+1	1/2	1	0	0	1/2	1	0	4.07	398.12
K^{-}	$s\bar{u}$	493.677	−1	1/2	−1	0	0	−1/2	−1	0	4.07	398.12
K^{0}	$d\bar{s}$	497.611	0	1/2	1	0	0	−1/2	1	1	4.07	399.54
$\bar{K}^{0}$	$s\bar{d}$	497.611	0	1/2	−1	0	0	1/2	−1	−1	4.07	399.54
	HIGH-MASS η MESONS ($J^P = 0^-$)											
$\eta_c(1s)$	$c\bar{c}$	2983.9	0	0	0	0	0	0	0	0	0.0874	443.9
$\eta_b(1s)$	$b\bar{b}$	9398.7	0	0	0	0	0	0	0	0	0.124	1038.7
	D MESONS ($J^P = 0^-$)											
D^{+}	$c\bar{d}$	1869.61	+1	1/2	0	1	0	1/2	1	0	0.234	594.9
D^{0}	$c\bar{u}$	1864.84	0	1/2	0	1	0	−1/2	1	1	0.233	592.7
D_s^{+}	$c\bar{s}$	1968.30	+1	0	1	1	0	0	2	1	0.230	604.9
D_s^{-}	$s\bar{c}$	1968.30	−1	0	−1	−1	0	0	−2	−1	0.230	604.9
	B MESONS ($J^P = 0^-$)											
B^{+}	$u\bar{b}$	5279.34	+1	1/2	0	0	1	1/2	1	0	0.262	1097.2
B^{0}	$d\bar{b}$	5279.65	0	1/2	0	0	1	−1/2	1	1	0.262	1095.0
B_s^{0}	$s\bar{b}$	5366.88	0	0	−1	0	1	0	0	0	0.256	1093.5
B_c^{+}	$c\bar{b}$	6274.9	+1	0	0	1	1	0	2	1	0.123	824.9

Table 4. *Cont.*

Particle Symbol	Quark Content	Rest Mass M (MeV)	Q (e)	I	S	C	B'	I_3	Y	Q'	BF	MD (MeV)
VECTOR MESONS ($J^P = 1^-$)												
ρ^+	$u\bar{d}$	775.11	+1	1	0	0	0	1	0	−1	85.5	768.28
ρ^-	$d\bar{u}$	775.11	−1	1	0	0	0	−1	0	1	85.5	768.28
ρ^0	$\frac{u\bar{u}-d\bar{d}}{\sqrt{2}}$	775.26	0	1	0	0	0	0	0	0	85.6	768.43
ω	$\frac{u\bar{u}+d\bar{d}}{\sqrt{2}}$	782.66	0	0	0	0	0	0	0	0	86.4	775.83
K^{*+}	$u\bar{s}$	891.66	+1	1/2	1	0	0	1/2	1	0	8.15	796.10
K^{*0}	$d\bar{s}$	895.81	0	1/2	1	0	0	−1/2	1	1	8.13	797.74
ϕ	$s\bar{s}$	1019.461	0	0	0	0	0	0	0	0	4.46	832.7
J/ψ (1s)	$c\bar{c}$	3096.916	0	0	0	0	0	0	0	0	0.110	556.9
Υ (1s)	$b\bar{b}$	9460.30	0	0	0	0	0	0	0	0	0.132	1100.3
D^{*+}	$c\bar{d}$	2010.26	+1	1/2	0	1	0	1/2	1	0	0.289	735.6
D^{*0}	$c\bar{u}$	2006.96	0	1/2	0	1	0	−1/2	1	1	0.289	734.8
D_s^{*+}	$c\bar{s}$	2112.1	+1	0	1	1	0	0	2	1	0.284	748.7
B^{*+}	$u\bar{b}$	5325.2	+1	1/2	0	0	1	1/2	1	0	0.273	1143.0
B^{*0}	$d\bar{b}$	5325.2	0	1/2	0	0	1	−1/2	1	1	0.273	1140.5
B_s^{*0}	$s\bar{b}$	5415.4	0	0	−1	0	1	0	0	0	0.267	1142.0
B_c^{*+}	$c\bar{b}$	(6274.9)	+1	0	0	1	1	0	2	1	0.123	824.9

(⋆) All listed quantities are defined in Table 1.

A large part of the PDG hadron data, namely the baryon datasets and their resonances, were recently reviewed by Thiel et al. [5], who also provided an overview of the theoretical quantum chromodynamics (QCD) framework used to draw comparisons with the experimental measurements. The same framework also governs our meta-analysis of particle masses and quantum-state transitions during hadron decays. However, our approach is essentially a meta-analysis, in the sense that we explore the available PDG data, including both baryon and meson measurements, to uncover properties of these particles and their decays that may be buried in the experimental results.

In the process, we draw connections with a number of QCD results and parameters of the Standard Model (SM) [6,7], which are then used to support and justify the new patterns revealed by the data. Some examples borrowed from the quantities listed in Table 1 are the mass deficits (*MD*s), the binding factors (*BF*s), and the "strong charge" (Q').

- *MD* (also called "mass defect" [4]) describes the energy content of the strong field in each particle. In the ground states (nucleons and pions), *MD* is effectively the minimum total energy required to bind the valence (anti)quarks detected only by QCD [8–10].
- On the other hand, *BF* represents the fraction of the total energy that binds each individual valence quark in a particle (see Section 2.2 for details). In particles representing excitations and resonances, these energies are not sufficient to maintain the binding; thus, such particles undergo decays on very short timescales [1–3,5].
- The strong charge (Q') is the missing quantum number needed to complete the weight diagrams of the SM, as shown in Figures 1–3 below. It is instrumental in deconstructing, for the first time, the hypercharge Y into an EM (Q) and a "strong" (Q') component (i.e., $Y = Q + Q'$; see Section 4 for details).

Our investigation of the PDG data proceeds in the following steps:

In Section 2, we analyze the mass deficits (*MD*s) of various particle groups, and we show that they can be described by the same scaling factors ("binding factors" (*BF*s) in Tables 2–4) of the valence quarks in each group. We also illustrate that it is the rest masses (M) of the various particles in a group (as opposed to *MD*s) that, on average, show hints of regularity and quantization at low energies. Detailed maps of the discrete jumps in rest mass without averaging are presented in Appendix A.

In Section 3, we show that differences in the mass deficits (and the observed differences in rest energies) in nucleons and pions (listed under *MD* in Tables 2 and 4) are almost entirely due to the strong force neutralizing the two repulsive Coulomb components between quarks with the same polarity. These repulsions develop only in charged particles ($Q \neq 0$). As would be expected, the same explanation is not sufficient for higher-energy particles (excited and resonant states).

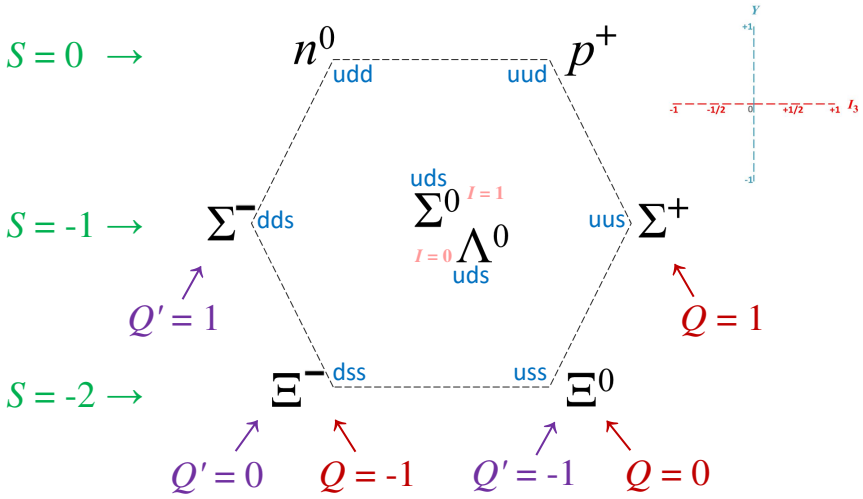

Figure 1. The weight diagram of the spin-parity ($J^{\mathrm{P}} = (1/2)^{+}$) baryon octet.

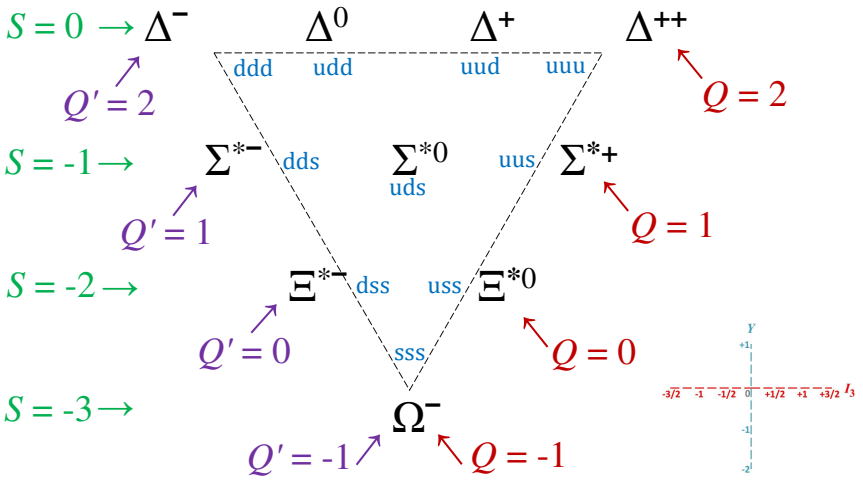

Figure 2. The weight diagram of the spin-parity ($J^{\mathrm{P}} = (3/2)^{+}$) baryon decuplet.

In Section 4, we introduce a combined quantum number ($Q' = Y - Q$), that represents the "strong piece" of the hypercharge (Y). This "strong charge" describes the SU(3) symmetry of particles along the right-leaning sides and diagonals of the various weight diagrams (e.g., Figures 1–3); Q' is conserved only in strong interactions in which Y is conserved, but it does not depend on Q, and it is the only quantum number (EM, weak, or strong) with a $(-1/3, 2/3)$ symmetry in each quark generation of increasing quark mass (Table 5).

In Section 5, we classify the most common hadron decays into strong, EM, and weak categories based on a single quantum number, the strong charge (Q'). This classification scheme is a new result, and it demonstrates the authority of this previously neglected (thus, inconspicuous, if at all known) quantum number, especially for particles that exhibit different types of decays in different channels.

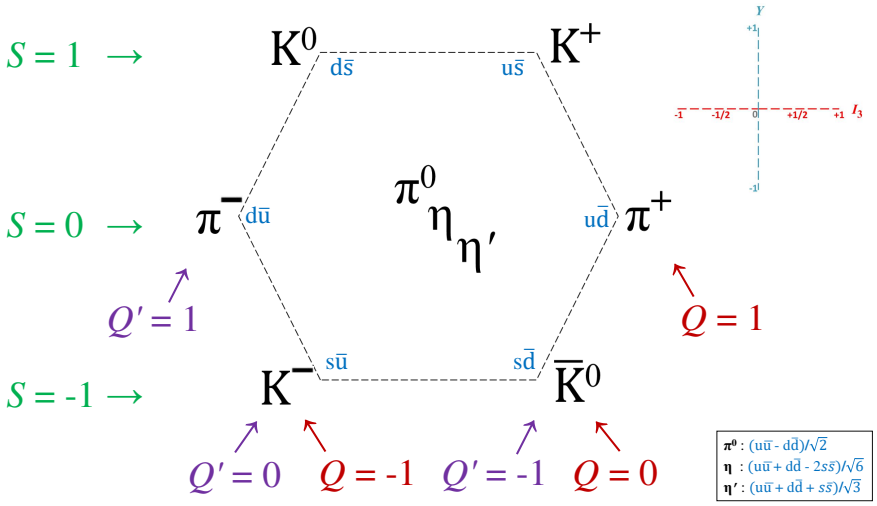

Figure 3. The weight diagram of the spin-parity $J^{\mathrm{P}} = 0^-$ pseudoscalar meson nonet.

Table 5. Rest masses, electric charge factors, and quantum numbers of quarks [⋆].

q =	u	d	s	c	b	t
Rest masses m_{q}	2.16 MeV	4.67 MeV	93.4 MeV	1.27 GeV	4.18 GeV	172.5 GeV
Electric charge factors ϑ_{e}	2	1	1	2	1	2
Quantum Numbers						
			All Interactions			
Q	2/3	−1/3	−1/3	2/3	−1/3	2/3
			Strong Interactions			
I_3	1/2	−1/2	0	0	0	0
Y	1/3	1/3	−2/3	4/3	−2/3	4/3
Q' [a]	−1/3	2/3	−1/3	2/3	−1/3	2/3
			Weak Interactions (Left-Chiral Quarks)			
$I_{3\mathrm{w}}$	1/2	−1/2	−1/2	1/2	−1/2	1/2
Y_{w}	1/3	1/3	1/3	1/3	1/3	1/3
Q'_{w} [b]	−1/3	2/3	2/3	−1/3	2/3	−1/3

[⋆] Rest masses are experimental averages taken from the 2022 PDG review [2]. Electric charge factors are described in Section 2.2. Quantum numbers are defined in Table 1. [a] No other quantum number, whether strong or weak, exhibits the u-d/s-c/b-t (−1/3, +2/3) symmetry seen in the strong charge ($Q' = Y - Q$) in each generation with increasing mass. [b] Weak charge ($Q'_{\mathrm{w}} \equiv Y_{\mathrm{w}}/2 - I_{3\mathrm{w}} = Y_{\mathrm{w}} - Q$); it does not exhibit the same symmetry as its strong counterpart (Q')—a fundamental distinction between the strong and the weak charge, although the EM charge (Q) couples to both of these charges in the same fashion.

In Section 6, we discuss our results, and we raise some new questions about the nature of the known hadrons. Some new calculations based on PDG data [1,2] that concern the energetics of valence (anti)quarks are described in Appendices B and C.

2. Particle Rest Masses, Mass Deficits, and Their Binding Factors

Particle rest masses (M) and mass deficits (MD) are listed in Tables 2–4 for baryons and mesons. All mass-related values are given in MeV. Quantities on the right of the broken vertical lines are derived from the data on the left of these lines. The definitions of all tabulated quantities are given in Table 1.

2.1. Rest Mass Jumps between Particle Groups

In Tables 2–4, the very few masses not yet measured in experiments but predicted by the SM [6] are listed in parentheses. It may not be as obvious in these listings, but rest masses of the low-energy states are effectively quantized in each of the three tables, although the rules differ between groups.

The weight diagrams of the low-energy states are shown in Figures 1–3, and the average quantization rules are shown in Figures 4–6. The detailed distributions of all individual energy jumps between states are quite crowded in all cases; they are shown in Appendix A (Figures A1–A3). The approximate energy jumps delineated from the data with increasing rest energy are as follows:

(1) $J^P = (1/2)^+$ baryons: 256 MeV and 128 MeV (Figures 4 and A1), although the smaller 121 MeV jump to Ξ^0 deviates from the rule for unknown reasons; also, the decay ($\Sigma^0 \to \Lambda^0 \gamma$) always emits a 77 MeV photon (γ), an important result that allows us to investigate the isospin content of Σ baryons in Appendix B.

(2) $J^P = (3/2)^+$ baryons: 150 MeV for all three jumps (Figures 5 and A2), although the smaller 139 MeV jump to Ω^- deviates from the rule for unknown reasons.

(3) $J^P = 0^-$ pseudoscalar mesons: 360 MeV and 50 MeV (Figures 6 and A3); the high-energy state (η'; not shown) lies 410 MeV above η, which, in turn, lies 410 MeV above the pionic ground state.

(4) $J^P = 1^-$ vector mesons ($\rho \to K^* \to \phi$): 120 MeV in both jumps (see Table 4).

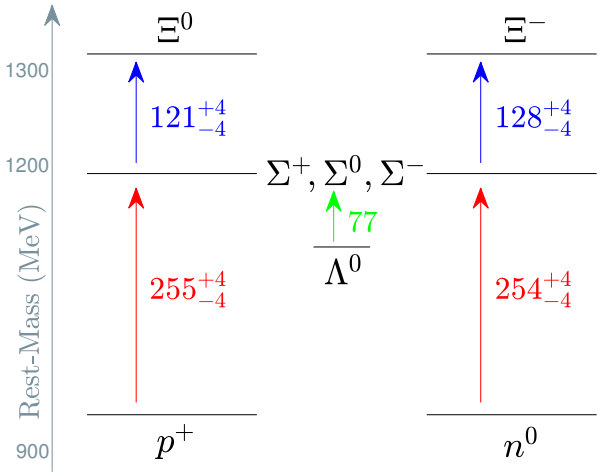

Figure 4. Average rest-mass energy levels for the $J^P = (1/2)^+$ baryons in Figure 1.

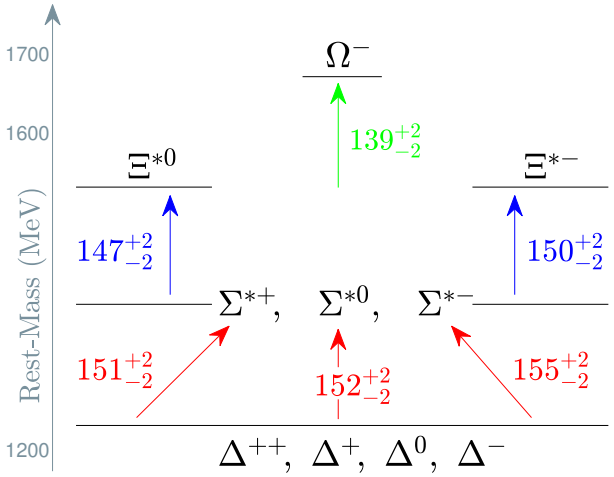

Figure 5. Average rest-mass energy levels for the $J^P = (3/2)^+$ baryons in Figure 2.

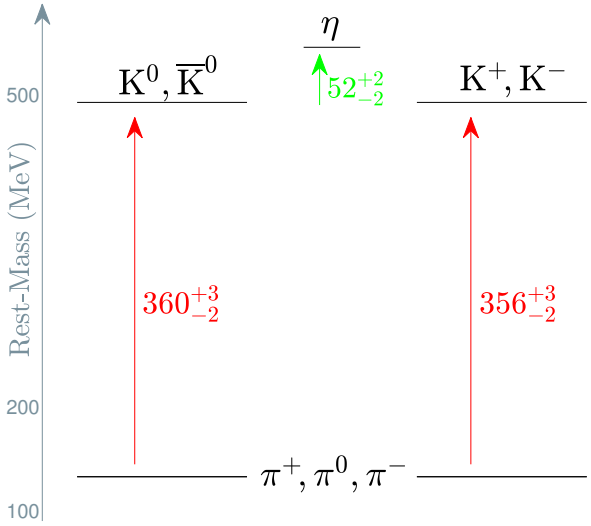

Figure 6. Average rest-mass energy levels for the $J^P = 0^-$ pseudoscalar meson nonet in Figure 3. The massive particle (η') is off scale; it lies 410 MeV above η which, in turn, lies 410 MeV above the pions. Also not shown, excitations $K^{*\pm}$ and K^{*0} lie 398 MeV above $K^\pm$ and K^0, respectively.

2.2. Mass Deficits and Binding Factors

Mass deficits and binding factors are listed in Tables 2–4 in columns *MD* and *BF*, respectively. *MD* values were obtained from the rest masses by subtracting the masses of the valence (anti)quarks, as shown in Table 1 (quark masses are listed in Table 5 below).

BF values were calculated from the corresponding *MD* values by assuming that (a) each (anti)quark is bounded by a "deficit" of rest energy proportional to its own rest-mass, (b) the scale factor (*BF*) is the same for all (anti)quarks confined to each particle, and (c) the relative factor of $\vartheta_e = 2$ in the electric charges of the (u, c, t) (anti)quarks is taken into account. Without the latter assumption, the *BF* values of the u and c quarks and their antiquarks would double, and the *BF* patterns seen in Tables 2–4 would not surface; in particular, the *BF* values would not be characteristically the same within each particle group.

As a case study, we describe the *BF* calculations for the nucleons, and we show how assumption (c) came into being. Initially, we set up two equations for the *MD*s of the nucleons, and we solved the system of equations to obtain the corresponding *BF*s. The two equations are

$$\begin{array}{l} \text{Proton} \quad (\text{uud}): \; 2m_u\, BF_u + \; m_d\, BF_d = MD_p \\ \text{Neutron}\,(\text{udd}): \; m_u\, BF_u + 2m_d\, BF_d = MD_n \end{array}, \tag{1}$$

where m_q is the mass of quark q (u or d) and the *MD* values for the proton and the neutron are $MD_p = M_p - 2m_u - m_d$ and $MD_n = M_n - m_u - 2m_d$, respectively. The two BF_q values of the solution are different and seemingly unrelated ($BF_u = 143.6$ and $BF_d = 66.16$), but when the fraction (f) of the constituent mass corresponding to each quark is calculated, the result is exactly $f = 1/3$ for all three quarks in both nucleons. This congruence implies that the above equations can be solved individually for a single (particle) binding factor, albeit scaling each of the u quarks by ϑ_e according to assumption (c). Thus, we solve the following equation for the proton scale (BF_p):

$$(2\vartheta_e m_u + m_d) BF_p = MD_p\,. \tag{2}$$

Then, we solve the following equation for the neutron scale (BF_n);

$$(\vartheta_e m_u + 2m_d) BF_n = MD_n\,. \tag{3}$$

The electric charge factor,

$$\vartheta_e = 2\,, \tag{4}$$

is applied to the u and c quarks (also to the t quark, which is too massive to be confined in hadrons; see Table 5 below), and we obtain $BF_p = 69.82$ and $BF_n = 67.94$. The small difference between these *BF*s is, in part, due to the slightly higher *MD* of the proton ($MD_p - MD_n = 1.22$ MeV), a value that does not appear in print as often as the famous difference in nucleonic masses ($M_p - M_n = -1.29$ MeV). We analyze these oppositely signed differences in Section 3 below.

3. Coulomb-Repulsion Origin of Mass-Deficit Differences in Nucleons and Pions

We adopt an elementary model of valence (anti)quark charges confined inside a particle, and we estimate the potential of the repulsive Coulomb-force components to do work if they are not suppressed in the bound state. Naturally, these repulsions are neutralized by work done by the strong force, which then constantly contributes an equal amount of energy to the *MD* of the particle. Attractive forces are ignored because they are not working to disrupt the particle. (Calculations of the total EM potential energy (*PE*) of the quarks in each of the particles depicted in Figures 7–9 below provide a crucial hint: $PE < 0$ and binding for both π^0 and n^0 but $PE \geq 0$ for $\pi^{\pm}$ and p^+.) The associated kinetic-energy content due to attractive forces is, of course, included in the *MD*s, along with the energy of the binding gluonic field and additional dynamical contributions from the so-called quark condensate and QCD trace anomaly [8–10].

We find that the simple electrostatic model shown in Figures 7–9 below describes, to a large extent, the small differences in the known *MD*s only for the ground states of nucleons and pions (Sections 3.1 and 3.2, respectively). All other states are highly energetic while they last, and the work done by the strong field against the repulsive Coulomb forces is just a small fraction of the corresponding *MD* differences. True to form, in Section 3.3, we demonstrate that Coulomb repulsion alone does not fully explain the measured *MD* differences in Σ^-/Σ^0 baryons with *MD* values ∼1090 MeV, differing by only 2.30 MeV; or in Ξ^-/Ξ^0 baryons with *MD* values of ∼1130 MeV, differing by only 4.34 MeV (Table 2 and Appendix B).

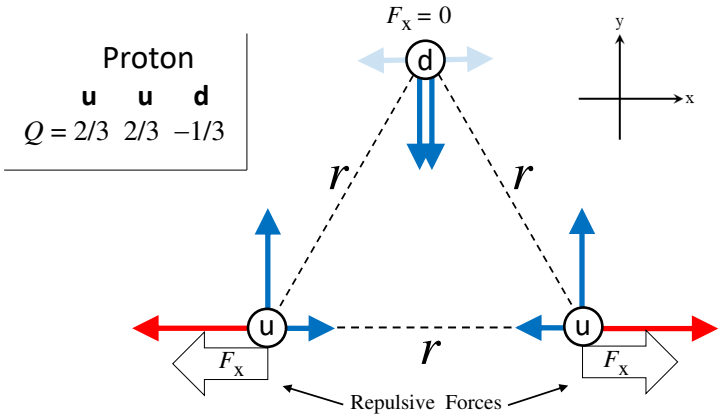

Figure 7. Repulsive Coulomb forces (F_x) between the $Q = +2/3$ u quarks in the proton. The relative magnitudes of the forces are drawn to scale (1:$\sqrt{3}$:2). Such repulsion does not develop between the $Q = -1/3$ d quarks in the neutron (Figure 8), which results in a higher mass deficit for the proton (+1.2167 MeV; top of Table 2). The typical distance (r) is assumed to be the same as the charge radius of the proton [11–15].

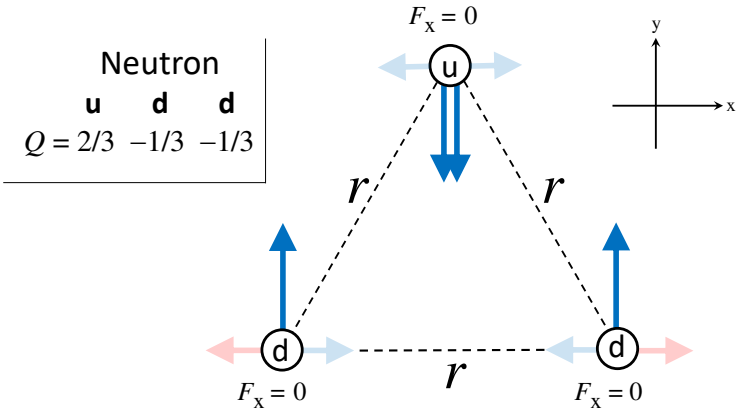

Figure 8. There are no repulsive Coulomb forces between the $Q = -1/3$ d quarks in the neutron, such as those between the u quarks in the proton (Figure 7). The relative magnitudes of the forces are drawn to scale ($1{:}\sqrt{3}$). The typical distance (r) is assumed to be the same as the charge radius of the proton [11–15].

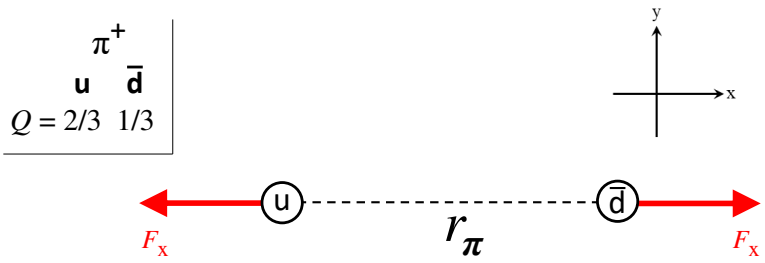

Figure 9. Repulsive Coulomb forces F_x between the u and $\bar{d}$ quarks in pion π^+. Such a repulsion does not develop in the mixed π^0 state $((|u\bar{u}\rangle - |d\bar{d}\rangle)/\sqrt{2})$, which results in a higher mass deficit for the $\pi^\pm$ pions (+4.59 MeV; top of Table 4). The typical distance (r_π) is much smaller than the charge radius of the proton [16], as discussed in the text.

3.1. Nucleons

The Coulomb forces between quarks in the proton and the neutron are drawn to scale in Figures 7 and 8, respectively. Faint arrows indicate components that cancel out. There are no repulsive components in the neutron. The resultant repulsive forces (F_x) in the proton are depicted by thick arrows.

For the characteristic side length (r) of the equilateral triangle shown in Figure 7, we adopt the charge radius of the proton [11–15] so that $r = 0.83$ fm (where 1 fm $= 10^{-15}$ m). Then, according to Coulomb's law, we find that $F_x \simeq 112$ Cb. The work that could be done by these two forces over distance r in the proton is then

$$W_p = 2rF_x \simeq 1.16 \text{ MeV}, \tag{5}$$

accounting for 95% of the difference ($MD_p - MD_n$) of 1.22 MeV seen in Table 2.

This estimate fares better than both the corresponding EM contribution determined from lattice computations of the mass difference between nucleons ($\Delta N_{QED} = 1.00 \pm 0.21$ MeV; see Table 1 in Ref. [17]) and the EM contribution determined from the Cottingham formula for virtual elastic Compton forward scattering [18–23]. In the latter case, any contribution from the inelastic region is negligible in a full QCD treatment [21–23], and the various estimates range from the recent value of 0.58 ± 0.16 MeV to 1.04 ± 0.35 MeV, falling around the original 50-year-old estimate of 0.76 ± 0.30 MeV [18]. Most of these accepted results are summarized in the 2016 review article of Leutwyler [24]. A much higher estimate of

1.30 ± 0.47 MeV [25] has been rejected because the ansatz used for the so-called subtraction function was found to be inconsistent with the short-range properties of QCD [19–21].

Based on the above theoretical values of the past produced by lattice QCD simulations and the Compton-scattering Cottingham formalism, we conclude that the best case raised for the fundamental EM value of $MD_{\rm p} - MD_{\rm n}$ is about 1 MeV, that is, ~82% of the measured value of 1.22 MeV. This is reason enough for our rudimentary Coulombic estimate of 1.16 MeV (Equation (5) above) to not be taken lightly, much less discounted in the face of more sophisticated calculations.

3.2. Pions

The repulsive Coulomb forces between the u and $\bar{\rm d}$ quarks in the positively charged pion (π^+) are shown in Figure 9. The same forces also appear in π^- but not in the neutral state (π^0). In Figure 9, the distance (r_π) between the quarks is taken to be the characteristic size of the pion, which is not known and is expected to be very small and 'nearly point-like' [16]. The problem is that the measured charge radius of $\pi^\pm$ (0.53–0.66 fm; Refs. [16,26]) is mostly due to a dominant ρ^0 resonance intervening in the annihilation process ($e^+ e^- \rightarrow \gamma \rightarrow \pi^+ \pi^-$) that also affects the size of the proton but not nearly as much (Ref. [16], Chapter 1, and Ref. [27]).

Therefore, we need to estimate the typical distance (r_π) between the quark and the antiquark in $\pi^\pm$ pions, and this determination requires some new assumptions. First, it is not reasonable to scale the nucleons down to the pions by assuming that the energy density of the binding field is the same in the two states. This is because the pions are quite different and much smaller than all other hadrons—the lowest-energy excitation of the vacuum [16] and a ground state for the mesons. (Such an attempt would yield a pion size of 0.35–0.44 fm, which is unacceptably large.) On the other hand, the pions contain only two point-like quarks that are presumably connected by a string in modern theories at the intersection of QCD and superstring theory [28–33]. Then, it seems reasonable to assume that it is the *mass per unit length* between two quarks that is about the same in nucleons and pions. With this assumption, we find that $r_\pi = 0.125$ fm in Figure 9 and, according to Coulomb's law, that $F_{\rm x} \simeq 3300$ Cb. The work that could be done by these two forces over a distance of r_π in the charged pions is then

$$W_{\pi^\pm} = 2 r_\pi F_{\rm x} \simeq 5.14 \text{ MeV}, \tag{6}$$

i.e., 12% larger than the ($MD_{\pi^\pm} - MD_{\pi^0}$) difference of 4.59 MeV seen in Table 4. The disagreement is entirely due to our rough estimate of r_π, and it would disappear for a comparable (ad hoc) value of $r_\pi = 0.14$ fm.

3.3. Σ^-/Σ^0 and Ξ^-/Ξ^0 Baryons

The $\Sigma^\pm$ baryons are charged excitations of the nucleons ($\Sigma^\pm \rightarrow n^0 \pi^\pm$ and $\Sigma^+ \rightarrow p^+ \pi^0$) [1,2]. In contrast, the Σ^0 baryon is an excitation of the Λ^0 resonance ($\Sigma^0 \rightarrow \Lambda^0 \gamma$), which is, itself, a nucleonic excitation. Although the Σ^+/Σ^0 *MD*s are comparable (Table 2), $MD_{\Sigma^+} < MD_{\Sigma^0}$ by 0.76 MeV. The neutral particle not having the lowest *MD* within its group is a singular property of only five excited states; in particular, it occurs in $\Sigma^{0,+}$ ($\delta_{MD} = 0.76$ MeV) and $\Xi_{\rm c}^{0,+}$ ($\delta_{MD} = 0.40$ MeV) baryons (Table 2); and in $\rm K^{0,\pm}$ ($\delta_{MD} = 1.42$ MeV), $\rho^{0,\pm}$ ($\delta_{MD} = 0.15$ MeV), and $\rm K^{*0,+}$ ($\delta_{MD} = 1.64$ MeV; see also Appendix B) mesons (Table 4). The same effect may also be realized in $\Delta^{0,-}$ baryons whose rest-masses are not sufficiently precise (Table 3).

On the other hand,

$$MD_{\Sigma^-} - MD_{\Sigma^0} = 2.30 \text{ MeV}. \tag{7}$$

This difference is not mostly the result of suppression of repulsive Coulomb forces between the dds valence quarks in Σ^- (the uds quarks in Σ^0 do not develop repulsive forces in our simple model, as shown in Figure 8 for the neutron). We demonstrate this by estimating

the work that could be done in Σ^- over a distance of r by the three repulsive forces (F_R) between the dds quarks (all Coulomb forces are repulsive, since all charges are negative).

Again, we adopt the simple triangular baryonic configuration as in Section 3.1. Since Σ^- is a nucleonic excitation, we adopt $r = 0.83$ fm here as well. Scaling based on equal linear mass densities would produce 1.06 fm and a smaller Coulombic contribution to the *MD* difference. With these assumptions, we find that $F_R \simeq 64.5$ Cb for the repulsive Coulomb force at each vertex of the equilateral triangle. The work that could be done by these forces over a distance of r in the Σ^- baryon is then

$$W_{\Sigma^-} = 3rF_R = 1.00 \text{ MeV}, \tag{8}$$

which is 43.5% of the *MD* difference shown above in Equation (7).

The above estimates also apply to the Ξ baryons (excitations of Λ^0 with $MD_{\Xi^-} - MD_{\Xi^0} = 4.34$ MeV; Table 2), in which the three Ξ^-(dss) valence quarks carry the same negative charge as the dds quarks in Σ^-, whereas Ξ^0(uss) shows no repulsive Coulomb forces in this model. Thus, $W_{\Xi^-} = 1.00$ MeV (as in Equation (8) for Σ^-), and this amounts to 23% of the measured *MD* difference of 4.34 MeV.

It is interesting to note that the EM content is identical between the Ξ^- and Σ^- excitations, whereas Σ^+ has the same EM content as the ground state (p^+). As a consequence, the Coleman–Glashow mass condition [34] (which is presently verified to achieve better than 1% accuracy) is valid for mass deficits as well, i.e.,

$$MD_{\Xi^-} - MD_{\Xi^0} = (MD_{\Sigma^-} - MD_{\Sigma^+}) + (MD_p - MD_n), \tag{9}$$

where the quark masses cancel out, and their charge distributions are the same between the two sides of the equation (see also Figures 1 and 4).

The results described in this section allow for a deep and thorough examination of the energy content of the Σ and Ξ excitations from the nucleonic ground state and the Λ^0 resonance, respectively. We present a detailed analysis in Appendix B.

4. The Inconspicuous Strong Charge (Q')

The third component (I_3) of isospin (I) and the hypercharge (Y) (Tables 2–4) are conserved in strong interactions (see also Section 5 for examples). These values are related to the always-conserved EM charge (Q) by the NNG formula [35–37].

$$Q = Y/2 + I_3\,. \tag{10}$$

Unlike Q, the hypercharge (Y) is not an actual EM charge, since this equation also involves the I_3 isospin component. The next question, then, is what do we get in place of Q when we flip the sign of I_3 in Equation (10)? Apparently, we get a supplementary charge (Q') such that

$$Q' \equiv Y/2 - I_3\,; \tag{11}$$

then, by adding Equations (10) and (11), we find that

$$Q + Q' = Y\,. \tag{12}$$

Therefore, Q' is the supplement of Q in strong interactions, and it is independent of the EM charge (Q), unlike the hypercharge (Y).

Charges Q and Q' are true opposites only for the following charged $Y = 0$ particles: $\Sigma^\pm$ and $\Sigma_b^\pm$; $\Sigma^{*\pm}$ and $\Sigma_b^{*\pm}$; and $\pi^\pm$ and $\rho^\pm$ (Tables 2–4). All other $Y = 0$ particles are at the centers of their weight diagrams, and they have $Q = Q' = 0$ (e.g., Σ^0, Σ^{*0}, and π^0 in Figures 1–3). In the general case with $Y \neq 0$, the strong charge (Q') is *the translation of the EM* (Q) across the Y axis (where $I_3 \equiv 0$).

The strong charge (Q') is conserved in strong decays, in which both Y and I_3 are also conserved individually (see Section 5 for a classification of strong/EM versus weak decays

based on Q'). We finally rewrite Equation (12) (and we calculate Q' in Tables 2–5) in the following convenient form:

$$Q' = Y - Q, \tag{13}$$

with the stipulation that Q' is equivalent to one of the well-known quantum numbers (Q, I_3, or Y) governing the strong and EM interactions. Finally, we identify Q' as the quantum number that remains constant along the *right-leaning sides/diagonals* in the weight diagrams depicted in Figures 1–3 above.

It may seem that Q' is redundant, but it is not. We describe two examples that show its efficacy as follows:

(a) In some kaon decays, $K^{\pm}$ and $K^0/\overline{K}^0$ can produce three pions via the reactions of $K^{\pm} \to \pi^+ \pi^- \pi^{\pm}$ and $K^0/\overline{K}^0 \to 3\pi^0$, respectively [1,2]. The only quantum number that differentiates charged from neutral kaon decays is Q', which switches from $0 \to \pm 1$ and from $\pm 1 \to 0$, respectively (see Table 4). No other quantum number can capture such oppositely directed transitions in these two types of weak decays of the K triplet. We revisit kaon decays in Appendices B and C.

(b) In quarks (Table 5), Q' is the only quantum number (among EM, strong, and weak numbers) that exhibits a repetitive $Q' = (-1/3, +2/3)$ pattern with increasing quark mass in each generation. This is a notable property, especially since for the EM charge (Q), the $(-1/3, +2/3)$ pattern breaks down in the first-generation (u, d) quarks.

Another example demonstrating an inconspicuous property of the strong charge (Q') is described in context in Section 5.6 below (EM versus strong decays).

5. Strong/Em Decays Based on Q' Conservation

In this section, we delineate the strong/EM decays by monitoring the strong charge (Q') (instead of using I_3 or Y) throughout several common and unusual decays of baryons and mesons, in which the EM charge (Q) is, of course, always conserved. When Q' is conserved, well-known numbers I_3 and Y are automatically conserved as well (yet they cannot distinguish strong from EM decays without help from total isospin (I), which is not conserved in EM decays).

This one-parameter Q' classification singles out the weak interactions too, just as Y or I_3 commonly do. Below, we use Q' to fist separate the weak decays from all other decays; then, we formulate an additional distinction that the absolute value of $|Q - Q'|$ offers, which appears to be capable of separating strong from EM decays as well.

5.1. $J^P = (1/2)^+$ *Baryon Octet*

These baryons are listed at the top of Table 2 and illustrated in Figure 1. In Table 6, we show their strong/EM decays in which Q' is conserved. We also categorize their excited and resonant states in the notes.

5.2. $J^P = (3/2)^+$ *Baryon Decuplet*

These baryons are listed at the top of Table 3 and illustrated in Figure 2. In Table 7, we show their strong/EM decays in which Q' is conserved. We also categorize their higher-energy states in the notes.

5.3. $J^P = 0^-$ *Pseudoscalar Meson Nonet*

These mesons are listed at the top of Table 4 and illustrated in Figure 3. In Table 8, we show their strong/EM decays in which Q' is conserved. We also categorize their excited and resonant states in the notes.

5.4. $J^P = 1^-$ Vector Meson Nonet

The vector mesons are listed at the bottom of Table 4. In Table 9, we show some typical strong/EM decays of the SU(3) nonet [1,2] in which Q' is conserved. This group contains particles such as ρ, ϕ, ω, and K^*. We also categorize their higher-energy states in the notes.

5.5. Summary of Tables 6–9

We summarize the material in Tables 6–9 as follows:

(1a) The $J^P = (1/2)^+$ baryon octet shows virtually no strong decays. Only Σ^0(uds) decays via photon emission (pions are not produced), and the proton does not decay at all. All other decays are due to weak interactions, and they all characteristically produce pions or leptons (see top of Table 6).

(1b) Higher-energy $J^P = (1/2)^+$ baryon states do reveal strong interactions, except Λ_c^+(udc) and Ω_c^0(ssc) (see bottom of Table 6). On the other hand, Λ_b^0(udb) shows both types of decay in different channels (see notes in Table 6).

(2) The $J^P = (3/2)^+$ baryons all show strong decays, except one, namely the Ω^-(sss) excitation (Table 7), which also exhibits some unique properties (strangeness: $S = -3$, $Y = -2$, $I = 0$) but not an unusual value of $Q' = -1$ (see Table 3).

(3a) In the $J^P = 0^-$ meson group, the pions show strong/EM decays, but the kaons show only weak decays (Table 8). At higher energies, the D and B mesons show very few strong/EM decays.

(3b) In the $J^P = 1^-$ group, all vector mesons with rest masses below 1020 MeV show strong/EM decays (Table 9). At higher energies, the decays are all strong/EM as well, with the striking exception of $D_s^{*+}(c\bar{s})$, which exhibits two uncommon properties ($Y = +2$, $I = 0$) but not unusual values of $S = +1$ and $Q' = +1$ (see Table 4).

Table 6. Strong/EM $J^P = (1/2)^+$ baryon modes (referring to the octet listed at the top of Table 2) and mean lifetimes (*ML*) in seconds.

Decay	Q'	*ML* (s)
The only strong/EM decay in the octet is		
$\Sigma^0 \to \Lambda^0 \gamma_{(77\,\mathrm{MeV})}$	$0 \to 0\,0 = 0$	7.4×10^{-20}
All other octet decays go to pions/leptons and are weak, e.g.,		
$n^0 \to p^+ e^- \bar{\nu}_e$	$1 \to 0\,0\,0 = 0$	878.4
$\Sigma^+ \to p^+ \pi^0$	$-1 \to 0\,0 = 0$	8.0×10^{-11}
$\Xi^- \to \Lambda^0 \pi^-$	$0 \to 0\,1 = 1$	1.6×10^{-10}
NOTES:		
Higher-energy states do show strong/EM decays, e.g.,		
$\Sigma_c^0 \to \Lambda_c^+ \pi^-$	$2 \to 1\,1 = 2$	3.6×10^{-22}
$\Omega_b^- \to \Omega^- J/\psi$	$-1 \to -1\,0 = -1$	1.6×10^{-12}
$\Lambda_b^0 \to \Lambda_c^+ D_s^-$	$0 \to 1\,-1 = 0$	1.5×10^{-12}
but Λ_c^+ and Ω_c^0 are noted for not having strong/EM decays		
$\Lambda_c^+ \to \Lambda^0 \pi^+ \eta$	$1 \to 0\,-1\,0 = -1$	2.0×10^{-13}
$\Omega_c^0 \to \Xi^0 K^- \pi^+$	$0 \to -1\,0\,-1 = -2$	2.7×10^{-13}
and Λ_b^0 is noted for also having some weak decays, e.g.,		
$\Lambda_b^0 \to p^+ D^0 \pi^-$	$0 \to 0\,1\,1 = 2$	1.5×10^{-12}
or with a K^- emitted in place of π^- (then, $Q' = 0 \to 1$).		

Table 7. Strong/EM $J^P = (3/2)^+$ baryon modes (referring to the decuplet listed at the top of Table 3) and mean lifetimes (*ML*) in seconds.

Decay	Q'	*ML* (s)
All decuplet decays are strong/EM, e.g.,		
$\Delta^{++} \to p^+ \pi^+$	$-1 \to 0\,-1 = -1$	5.6×10^{-24}
$\Delta^- \to n^0 \pi^-$	$2 \to 1\,1 = 2$	5.6×10^{-24}
$\Sigma^{*-} \to \Lambda^0 \pi^-$	$1 \to 0\,1 = 1$	1.7×10^{-23}
$\Xi^{*0} \to \Xi^- \pi^+$	$-1 \to 0\,-1 = -1$	7.2×10^{-23}
$\Xi^{*0} \to \Xi^0 \pi^0$	$-1 \to -1\,0 = -1$	7.2×10^{-23}

Table 7. *Cont.*

Decay	Q'	*ML* (s)
except for Ω^- (which is quite long-lived), e.g.,		
$\Omega^- \to \Lambda^0\,K^-$	$-1 \to 0\,0 = 0$	8.2×10^{-11}
NOTES:		
All higher-energy states also show strong/EM decays, e.g.,		
$\Sigma_c^{*0} \to \Lambda_c^+\,\pi^-$	$2 \to 1\,1 = 2$	4.3×10^{-23}
$\Sigma_b^{*+} \to \Lambda_b^0\,\pi^+$	$-1 \to 0\,-1 = -1$	7.0×10^{-23}
$\Xi_c^{*0} \to \Xi_c^+\,\pi^-$	$1 \to 0\,1 = 1$	2.8×10^{-22}
$\Xi_b^{*0} \to \Xi_b^-\,\pi^+$	$-1 \to 0\,-1 = -1$	7.3×10^{-22}
$\Omega_c^{*0} \to \Omega_c^0\,\gamma_{(70.7\,\mathrm{MeV})}$	$0 \to 0\,0 = 0$	Unknown

Table 8. Strong/EM $J^P = 0^-$ pseudoscalar meson modes (referring to the nonet listed at the top of Table 4) and mean lifetimes (*ML*) in seconds.

Decay	Q'	*ML* (s)
Some pion decays and the η, η' decays are strong/EM, e.g.,		
$\pi^0 \to (2\gamma)_{(135\,\mathrm{MeV})}$	$0 \to 0\,0 = 0$	8.5×10^{-17}
$\eta \to \pi^+\,\pi^0\,\pi^-$	$0 \to -1\,0\,1 = 0$	5.0×10^{-19}
$\eta' \to \pi^+\,\pi^-\,\eta$	$0 \to -1\,1\,0 = 0$	3.3×10^{-21}
$\eta' \to \rho^0\,\gamma_{(182.5\,\mathrm{MeV})}$	$0 \to 0\,0 = 0$	3.3×10^{-21}
Kaon decays are weak, e.g.,		
$K^+ \to \mu^+\,\nu_\mu$	$0 \to -1\,0 = -1$	1.2×10^{-8}
$K^0_{(L)} \to 3\pi^0$	$1 \to 0\,0\,0 = 0$	5.1×10^{-8}
NOTES:		
Higher-energy states (D and B mesons) show but a few strong/EM decays, viz.,		
$D^+ \to K^0\,\pi^+$	$0 \to 1\,-1 = 0$	1.0×10^{-12}
$B^+ \to K^0\,\pi^+$	$0 \to 1\,-1 = 0$	1.6×10^{-12}
$B_s^0 \to J/\psi\,\pi^+\,\pi^-$	$0 \to 0\,-1\,1 = 0$	1.5×10^{-12}
$B_c^+ \to D_s^+\,\phi$	$1 \to 1\,0 = 1$	4.5×10^{-13}
The famous production of Ω^- [38,39] is strong, viz.		
$K^-\,p^+ \to \Omega^-\,K^+\,K^0$	$0\,0 \to -1\,0\,1 = 0$	
but subsequent decays are weak, i.e., $K^0 \to \pi^+\,\pi^-$ ($Q' = 1 \to 0$) and $\Omega^- \to \Lambda^0\,K^-$ ($Q' = -1 \to 0$).		
It is interesting that kaons are produced in strong decays but then decay only via the weak interaction.		

Table 9. Strong/EM $J^P = 1^-$ vector meson modes (referring to the $(\rho, \phi, \omega, K^*)$ nonet listed in the lower part of Table 4) and mean lifetimes (*ML*) in seconds.

Decay	Q'	*ML* (s)
All nonet decays are strong/EM, e.g.,		
$\rho^+ \to \pi^+\,\pi^0$	$-1 \to -1\,0 = -1$	4.4×10^{-24}
$\rho^- \to \pi^-\,\eta$	$1 \to 1\,0 = 1$	4.4×10^{-24}
$\rho^0 \to \pi^+\,\pi^-$	$0 \to -1\,1 = 0$	4.5×10^{-24}
$\omega \to \pi^+\,\pi^0\,\pi^-$	$0 \to -1\,0\,1 = 0$	7.8×10^{-23}
$\phi \to K^+\,K^-$	$0 \to 0\,0 = 0$	1.5×10^{-22}
$K^{*+} \to K^0\,\pi^+$	$0 \to 1\,-1 = 0$	3.3×10^{-23}
$K^{*0} \to K^+\,\pi^-$	$1 \to 0\,1 = 1$	1.4×10^{-23}
NOTES:		
Higher-energy states (D^* and B^* mesons) show strong/EM decays in almost all cases, e.g.,		
$D^{*+} \to D^0\,\pi^+$	$0 \to 1\,-1 = 0$	7.9×10^{-21}
$B_s^{*0} \to B_s^0\,\gamma_{(48.6\,\mathrm{MeV})}$	$0 \to 0\,0 = 0$	Unknown
except for a striking exception, namely the weak decay		
$D_s^{*+} \to D^{*+}\,\pi^0$	$1 \to 0\,0 = 0$	$> 3.4 \times 10^{-22}$
or with a photon $\gamma_{(101.8\,\mathrm{MeV})}$ emitted in place of π^0.		

5.6. Electromagnetic versus Strong Decays

It is generally observed that EM decays do not conserve total isospin (I), which is a distinction from strong decays [38,40]. Although this statement is essentially correct, the implied separation is imprecise and needs to be refined (by monitoring Q' instead of I), as there are very few decays that get misclassified by total isospin.

(a) Decays of the $\rho \to \pi\,\pi$ type (where $Q = 0 \to 0\,0$ is the only one not allowed) are said to be strong [38], although total isospin is clearly not conserved (all three particles have $I = 1$; Table 4).

(b) Decays of the Δ baryons are said to be strong [38], as they all conserve total isospin. But Δ^+ and Δ^0 each show two decay channels, so it becomes hard to argue that the strong force somehow cannot settle into one preferred mode of decay in driving these resonances back to their ground states.

We revisit these exceptional cases in Section 5.6.2 below, where we apply a new methodology based on the absolute value of $|Q - Q'|$ that we formulate first in Section 5.6.1.

5.6.1. The Important Role of the Absolute Difference ($|Q - Q'|$).

EM charge (Q) is conserved in all hadron decays, signifying that EM forces are always present in particle reactions. Here, we search the 31 strong/EM decays listed in Tables 6–9, and we identify the predominant EM decays based only on the behavior of the strong charge (Q') (along with the always-visible EM charge Q), that is, without relying on the (non-)conservation of isospin (I) at all. The resulting classification of reactions is summarized in the three cases listed in Table 10.

The EM versus strong classification scheme in Table 10 stems from the following principle. Eliminating Y between Equations (10) and (11), we determine I_3 in terms of the difference between the two charges, viz.,

$$I_3 = \frac{1}{2}(Q - Q')\,, \tag{14}$$

which, of course, shows that I_3 is conserved in strong and EM decays, in which the two charges are conserved. But predominantly strong interactions should also require the conservation of the magnitude ($|I_3|$), a number that is not conserved in EM interactions. In effect, here, we disregard the term $\left(I_1^2 + I_2^2\right)$, which is not fully deterministic (according to the uncertainty principle), when a (strong) state has a definite value of the I_3 component [41]. Therefore, the two types of non-weak decays should be distinguishable based on $|I_3|$ alone. To this end, the factor of $1/2$ in Equation (14) is not needed, which allows us to finally monitor only the "distance" between the two charges, viz.,

$$|Q - Q'| \;\equiv\; \sqrt{(2I_3)^2} \;=\; 2|I_3|\,, \tag{15}$$

in the 31 examples of strong/EM decays listed in Table 10.

In Table 10, the decays grouped together in Cases 2 and 3 (predominantly strong (ST) and predominantly EM decays, respectively) are classified on the basis of nonzero $|Q - Q'|$ values, precisely as would also be expected from the (non-)conservation of I. On the other hand, the EM decays of Case 1 (with $|Q - Q'| \equiv 0$ across each reaction) hold some surprises.

(a) Reactions emitting photons reveal their primarily EM nature, as do reactions emitting neutral vector mesons (ω, ϕ, or J/ψ(1s)—but not $\Upsilon(1s)$, whose enormous 9.46-GeV rest mass trumps that of all the other particles).

(b) By showing their true EM nature, reactions with $|Q - Q'| \equiv 0$ (i.e., $I_3 \equiv 0$) teach us that in cases where $I_3 = 0$ across the entire decay reaction (i.e., $Q = Q' = Y/2$), (non-)conservation of I becomes practically irrelevant; then, the reaction is mediated primarily by the EM interaction.

(c) The decay of $\Lambda_b^0 \to \Lambda_c^+\,D_s^-$ produces a charged meson and a Λ_c^+, the only Λ particle that actually carries EM charge. This EM reaction also shows that $Q' = 0 \to 1\,-1 = 0$, which differentiates it from (i) the other $Q' = 0 \to 0\,0 = 0$ EM decays producing photons (see Case 1) and (ii) the Λ-producing Σ^* and Σ_c decays mediated by the strong interaction (see Case 2).

The decay of $\Lambda_b^0 \to \Lambda_c^+ D_s^-$ in item (c) represents one of many cases in which two opposite EM charges ($Q = 0 \to 1\ -1$) appear "out of nowhere" in the decay fragments; thus, the reaction must be characterized as naturally EM, irrespective of the behavior of its quantum numbers (although the weak force may also have a role in intermediate steps). On the other hand, $I = 0 \to 0\,0$, indicating that isospin conservation is not relevant here; an attempt to use "I-conservation" for $I \equiv 0$ across the reaction would lead to misclassification. Another conundrum appears in two of six Δ-baryon decay channels, which we analyze below.

Table 10. Classification of the 31 non-weak (Q'-conserving) decays from Tables 6–9 as strong (ST) or EM based on the behavior of the charge distance ($|Q - Q'|$) and corresponding mean lifetimes (*ML*) in seconds.

EM or ST?	Decay	Q'	$\lvert Q - Q' \rvert$	*ML* (s)
	CASE 1: $\lvert Q - Q' \rvert \equiv 0$ on the left side and across the entire decay reaction.			
	The 8 examples from Tables 6–9 are			
	$\Sigma^0 \to \Lambda^0 \gamma$	$0 \to 0\,0 = 0$	$0 \to 0\,0 = 0$	7.4×10^{-20}
	$\Omega_b^- \to \Omega^- J/\psi$	$-1 \to -1\,0 = -1$	$0 \to 0\,0 = 0$	1.6×10^{-12}
	$\Lambda_b^0 \to \Lambda_c^+ D_s^-$	$0 \to 1\ -1 = 0$	$0 \to 0\,0 = 0$	1.5×10^{-12}
	$\Omega_c^{*0} \to \Omega_c^0 \gamma$	$0 \to 0\,0 = 0$	$0 \to 0\,0 = 0$	Unknown
	$\pi^0 \to \gamma\,\gamma$	$0 \to 0\,0 = 0$	$0 \to 0\,0 = 0$	8.5×10^{-17}
	$\eta' \to \rho^0 \gamma$	$0 \to 0\,0 = 0$	$0 \to 0\,0 = 0$	3.3×10^{-21}
	$B_c^+ \to D_s^+ \phi$	$1 \to 1\,0 = 1$	$0 \to 0\,0 = 0$	4.5×10^{-13}
	$B_s^{*0} \to B_s^0 \gamma$	$0 \to 0\,0 = 0$	$0 \to 0\,0 = 0$	Unknown
EM	When $\lvert Q - Q' \rvert \equiv 0$ across the decay reaction, then $I_3 \equiv 0$, and it does not appear in the wave functions. Isospin (non-)conservation then becomes a meaningless distinction. Photon emission in many reactions also reveals their predominantly EM nature. Note: The *ML*s of Ω_b^-, Λ_b^0, and B_c^+ are long, so weak interactions are involved too.			
	CASE 2: $\lvert Q - Q' \rvert \neq 0$ on the left side and conserved across the reaction.			
	The 9 examples from Tables 6–9 are			
	$\Delta^{++} \to p^+ \pi^+$	$-1 \to 0\ -1 = -1$	$3 \to 1\,2 = 3$	5.6×10^{-24}
	$\Delta^- \to n^0 \pi^-$	$2 \to 1\,1 = 2$	$3 \to 1\,2 = 3$	5.6×10^{-24}
	$\Sigma^{*-} \to \Lambda^0 \pi^-$	$1 \to 0\,1 = 1$	$2 \to 0\,2 = 2$	1.7×10^{-23}
	$\Xi^{*0} \to \Xi^0 \pi^0$	$-1 \to -1\,0 = -1$	$1 \to 1\,0 = 1$	7.2×10^{-23}
	$\Sigma_c^0 \to \Lambda_c^+ \pi^-$	$2 \to 1\,1 = 2$	$2 \to 0\,2 = 2$	3.6×10^{-22}
	$\Sigma_c^{*0} \to \Lambda_c^+ \pi^-$	$2 \to 1\,1 = 2$	$2 \to 0\,2 = 2$	4.3×10^{-23}
	$\Sigma_b^{*+} \to \Lambda_b^0 \pi^+$	$-1 \to 0\ -1 = -1$	$2 \to 0\,2 = 2$	7.0×10^{-23}
	$\rho^+ \to \pi^+ \pi^0$	$-1 \to -1\,0 = -1$	$2 \to 2\,0 = 2$	4.4×10^{-24}
	$\rho^- \to \pi^- \eta$	$1 \to 1\,0 = 1$	$2 \to 2\,0 = 2$	4.4×10^{-24}
ST	When $\lvert Q - Q' \rvert \neq 0$ and is conserved in the decay, then $\lvert I_3 \rvert$ is also conserved. Then, the decay reaction is mediated primarily by the strong interaction. Note: All *ML*s are very short, a typical property of predominantly strong decays.			
	CASE 3: $\lvert Q - Q' \rvert \neq 0$ on at least one side and is not conserved across the reaction.			
	The 14 examples from Tables 7–9 are			
	$\Xi^{*0} \to \Xi^- \pi^+$	$-1 \to 0\ -1 = -1$	$1 \to 1\,2 = 3$	7.2×10^{-23}
	$\Xi_c^{*0} \to \Xi_c^+ \pi^-$	$1 \to 0\,1 = 1$	$1 \to 1\,2 = 3$	2.8×10^{-22}
	$\Xi_b^{*0} \to \Xi_b^- \pi^+$	$-1 \to 0\ -1 = -1$	$1 \to 1\,2 = 3$	7.3×10^{-22}
	$\eta \to \pi^+ \pi^0 \pi^-$	$0 \to -1\,0\,1 = 0$	$0 \to 2\,0\,2 = 4$	5.0×10^{-19}
	$\eta' \to \pi^+ \pi^- \eta$	$0 \to -1\,1\,0 = 0$	$0 \to 2\,2\,0 = 4$	3.3×10^{-21}
	$D^+ \to K^0 \pi^+$	$0 \to 1\ -1 = 0$	$1 \to 1\,2 = 3$	1.0×10^{-12}
	$B^+ \to K^0 \pi^+$	$0 \to 1\ -1 = 0$	$1 \to 1\,2 = 3$	1.6×10^{-12}
	$B_s^0 \to J/\psi\,\pi^+ \pi^-$	$0 \to 0\ -1\ 1 = 0$	$0 \to 0\,2\,2 = 4$	1.5×10^{-12}
	$\rho^0 \to \pi^+ \pi^-$	$0 \to -1\,1 = 0$	$0 \to 2\,2 = 4$	4.5×10^{-24}
	$\omega \to \pi^+ \pi^0 \pi^-$	$0 \to -1\,0\,1 = 0$	$0 \to 2\,0\,2 = 4$	7.8×10^{-23}
	$\phi \to K^+ K^-$	$0 \to 0\,0 = 0$	$0 \to 1\,1 = 2$	1.5×10^{-22}
	$K^{*+} \to K^0 \pi^+$	$0 \to 1\ -1 = 0$	$1 \to 1\,2 = 3$	3.3×10^{-23}
	$K^{*0} \to K^+ \pi^-$	$1 \to 0\,1 = 1$	$1 \to 1\,2 = 3$	1.4×10^{-23}
	$D^{*+} \to D^0 \pi^+$	$0 \to 1\ -1 = 0$	$1 \to 1\,2 = 3$	7.9×10^{-21}
EM	When $\lvert Q - Q' \rvert \neq 0$ on at least one side and is not conserved, then $\lvert I_3 \rvert$ is not conserved either. Then, the decay reaction is mediated primarily by the EM interaction. Note: The *ML*s of D^+, B^+, and B_s^0 are long, so weak interactions are involved too.			

5.6.2. Decay Channels of ρ and Δ Resonances

(a) Based on the $|Q - Q'|$ criterion, the primary modes of $\rho^{\pm}$ are strong (ST), but the decay of the neutral ρ^0 to charged pions is EM (Table 10). Since $Y = 0$ for all particles involved, $Q' = -Q$; thus, the strong charge is obviously conserved in all of these decays. But the charge distance ($|Q - Q'| = 2|Q|$) is not conserved in the ubiquitous decay of $\rho^0 \to \pi^+ \pi^-$, telling us that this is an EM reaction (Case 3 in Table 10).

(b) The decays of Δ^{++} and Δ^-, as well as the primary decays of Δ^+ and Δ^0 down to their parental states (p^+ and n^0, respectively), are mediated by the strong interaction (Case 2 in Table 10 [38,40]), and they are not going to occupy us further. On the other hand, Δ^+ and Δ^0 have two additional decay channels in which they do not return to their parental states (p^+ and n^0, respectively), viz.,

$$\Delta^+ \to n^0\, \pi^+ \left(I = \tfrac{3}{2} \to \tfrac{1}{2}\, 1 = \tfrac{3}{2} \Rightarrow \text{ST};\ |Q - Q'| = 1 \to 1\, 2 = 3 \Rightarrow \text{EM} \right), \tag{16}$$

and

$$\Delta^0 \to p^+\, \pi^- \left(I = \tfrac{3}{2} \to \tfrac{1}{2}\, 1 = \tfrac{3}{2} \Rightarrow \text{ST};\ |Q - Q'| = 1 \to 1\, 2 = 3 \Rightarrow \text{EM} \right). \tag{17}$$

According to I conservation, these two reactions are thought to generally belong to the ST category, where all the other Δ decays also belong; however, $|Q - Q'|$ in Equations (16) and (17) disagrees and places them in the EM category.

Channel (16) cannot be judged at first sight, but channel (17) is yet another example of EM charges appearing "out of nowhere" in the two fragments. Thus, we suggest that these two decays are mediated primarily by the EM interaction (unlike the strong decays of $\Delta^+ \to p^+ \pi^0$ and $\Delta^0 \to n^0 \pi^0$) and that the (non-)conservation of the charge distance ($|Q - Q'|$) (Equation (15)) is the refinement needed to accurately distinguish between primarily EM and primarily ST decays.

6. Summary of Results and Open Questions

6.1. Summary of Results

In this work, we have presented a review and meta-analysis of some of the extensive hadron data painstakingly collected by the PDG members [1,2] over many years. In Section 2, we examined the rest masses and the mass deficits of the hadrons. We found that jumps in rest masses appear to be approximately quantized and that mass deficits (*MD*s) can be reconstructed from the masses of the valence quarks multiplied by the same binding factor (*BF*) in each hadron. We summarized our results in Figures 4–6 and in Tables 2–4.

In Section 3, we showed that small differences in the mass deficits of nucleons or pions (the identified ground states of baryons and mesons, respectively) can be explained by the suppression of the repulsive Coulomb forces by the strong field that binds these fundamental particles together in a highly dynamic environment. The mass-deficit differences of higher excitations and resonances cannot be explained in the same way; such higher energetic states are in possession of much more free energy (while they last) than that predicted by standard suppression of Coulombic repulsions.

In Section 4, we introduced a (long-overdue) charge, namely the "strong charge" (Q'); the quantum number (Q') is not a real charge (the strong field is charge-blind) but an imitation that describes the weight of the strong force among the various well-known quantum numbers, such as Q, I_3, and Y. We discovered Q' in the pre-eminent weight diagrams of low-energy hadrons (Figures 1–3) by asking an obvious (and long-overdue) question, namely which quantity remains invariant along the right-leaning sides and diagonals of the geometric figures depicted in these weight diagrams? The answer is the "strong" charge ($Q' = Y - Q$) (Equation (13)), a *translation* of the EM charge (Q) across the ($I_3 = 0$) Y axis, where I_3 is the third component of isospin (I) and Y is the hypercharge.

Based on the results presented in Section 5, the strong charge (Q') is expected to have a long future life. Not only is it as tall a peer to Y and I_3 (Equation (11)) in separating weak from strong/EM particle decays, but it can also help us distinguish predominantly

strong from predominantly EM decays with a little help from the (always visible in reactions) EM charge (Q). The absolute difference ($|Q - Q'|$) (Equation (15)) is conserved in strong reactions.

We deferred additional tortuous analyses to three appendices. In Appendix A, we present transition diagrams between the various excitations and resonances of the low-energy particles (Figures A1–A3). They appear to be too crowded to the eye, and this is why we also drew corresponding summarizing diagrams in Figures 4–6 above.

In Appendix B, we calculate the transition energies between the valence states in $\Sigma/\Lambda^0/\Xi/\Omega/\Xi^*$ baryons at the quark level. We determine the energy cost for lower-mass quarks (u, d, and for transformation to different quarks via the weak interaction. Perhaps the most important result is not the numerical values obtained for the various quark transitions (see, e.g., Equation (A7)) but the realization that an isospin change by $\delta I = +1/2$ does not carry the same cost during $I = 0 \to 1/2$ and $I = 1/2 \to 1$ transitions. In a quantum state with $I = 0$, isospin is not realized, and the $I = 0$ particle needs to be "paid" (a small amount of excitation energy) to be taught of the existence of nonzero isospin; thus, $I_{0\to 1/2} \gtrsim I_{1/2\to 1}$. By the same token, when $I_3 \equiv 0$ across a decay reaction (Case 1 in Table 10), the quantum states cannot possibly conserve zero isospin, a quantity that is obviously absent across the entire reaction.

In Appendix C, we turn to antimatter quarks in low-energy K and π pseudoscalar mesons. We calculate the antiquark transition energies, and we find, to our surprise, that they are very different from the quark energy levels in ordinary matter (Appendix B). In particular, we determine that $\bar{\mathrm{d}}$ is the lowest antiquark state (i.e., the ground state), as opposed to the well-known u-quark ground state in ordinary matter. The resulting (anti)quark transition diagrams are depicted side-by-side in Figure A4 for comparison purposes. As we discuss below, the results summarized in Appendix C form a platform for understanding the origin of CP violation.

6.2. Open Questions

Examining the main results of this meta-analysis, we do not see any obvious issues left open-ended for the future, except, possibly, for the minor disagreement over the predictions of I conservation and $|Q - Q'|$ conservation in the two alternative channels of Δ^+/Δ^0 decays (see Section 5.6.2); this issue deserves more consideration in the near future.

On the other hand, we wrap up this meta-analysis thinking about some not-so-obvious questions concerning how the binding factors and the (anti)quark transitions observed in low-energy particle decays relate to the coupling constants of the SM and the observed baryon asymmetry. Briefly, these open issues are summarized as follows:

(1a) Consider the binding factors (BF) of the nucleons listed at the top of Table 2 ($BF = 69.8$ and 67.9 for p^+ and n^0, respectively). Their sum, 137.7, is close (within 0.5%) to the reciprocal of the EM fine-structure constant ($\alpha = 1/137.036$) [3], i.e., the famous number $\alpha^{-1} \simeq 137$ [6,42]. Then, the average binding factor ($\overline{BF}_{\mathrm{q}} = 68.85$) of each quark in each nucleon appears to be very close to

$$\frac{\alpha^{-1}}{2} = 68.52\,. \tag{18}$$

It is not surprising that the fine-structure constant may be involved in the specification of the dimensionless binding factors. But the principles behind this identification, as well as the identifications that follow, are not yet known; thus, we cannot formally dismiss the possibility of a coincidence at this time. Nevertheless, the concurrences listed in items (1)–(3) are too many to be explained by a sequence of fortuitous events.

(1b) Consider next the binding factors (*BF*) of the pions listed at the top of Table 4 (*BF* = 14.8 for $\pi^{\pm}$). This *BF* value is close (within 0.4%) to half of the reciprocal of the weak-interaction coupling constant (α_w, i.e., $\alpha_w^{-1}/2$), where

$$\alpha_w = \frac{g_w^2}{4\pi} = \frac{1}{29.47}\,, \tag{19}$$

evaluated based on the gauge factor ($g_w = 0.653$) [6] of the weak interaction. It seems unavoidable that the fundamental coupling constants of the subatomic interactions are correlated with the binding factors of the ground states, the nucleons, and the pions.

(2a) The above identifications are also supported, to an extent, by the constituent quarks of the Δ baryons, which show, by far, the largest *BF* values among all elementary particles (Table 3). Their average binding factor ($\overline{BF}_q = 90.7$) for each individual quark is only 0.7% smaller than the "strong" value of

$$BF_{ST} = \frac{4}{3}\left(\frac{\alpha^{-1}}{2}\right) = 91.36\,. \tag{20}$$

For the BF_q values of these low-energy Δ resonances (just 293 MeV above the nucleons), the "strong" factor of 4/3 appears to be necessary in rescaling the well-known EM factor of $\alpha^{-1}/2$ (see Equation (18) above).

(2b) We identified the above strong factor of 4/3 with the quadratic Casimir charge (C_F) of the SU(3) fundamental representation. The Casimir charge ($C_F = 4/3$) commonly appears in SU(3) in strong interactions. For instance, it helps define the short-range term of the potential energy of the quarkonia $c\bar{c}$ and $b\bar{b}$ [7,43].
Therefore, by extension, it seems that all *BF*s listed in Tables 2–4 are related to the fundamental QCD couplings and their gauge factors in multifarious ways [6,7]. In such a case, the *BF* value for each particle reveals information about the constituent subatomic fields that support the current quarks and antiquarks in the dynamic environments they set up inside the particles.

(3) The small differences in *BF* values within the same state (or group of particles) are significant. They seem to be caused by the components of the strong field and the particular ways they use to bind each individual particle (or there are no differences in cases in which the *BF* values are identical within the same group; Tables 2–4). This conclusion stems from the following surprising congruence: the precise *BF* ratios of the Δ baryons and the nucleons are equal, viz.,

$$\frac{BF(\Delta^+)}{BF(\Delta^0)} = \frac{BF(p^+)}{BF(n^0)} = 1.028\,; \tag{21}$$

and the pionic ratio ($BF(\pi^+)/BF(\pi^0) = 1.033$) is not too different, although we used a value for $BF(\pi^0)$ that is only an approximation for the mixed neutral state (π^0).

(4a) It is generally believed that there are no asymmetries between quarks and antiquarks, and this belief has sparked many investigations toward understanding today's "baryon asymmetry", the complete dominance of matter over antimatter in the present universe [44–47]. On the other hand, results from the LHCb experiment [48] indicated a substantial asymmetry (CP violation) in the weak decay of $\Lambda_b^0 \to p^+\,\pi^-\,\pi^+\,\pi^-$ (last reaction in Table 6 with $D^0 \to \pi^-\pi^+$ in the final state; see also [49] for similar LHCb results in weak decays of the charmed D^0 meson).

(4b) In the course of our investigation, we uncovered a theoretical basis for CP violation in mesons. In Appendix C, we show that the energy levels of quarks and antiquarks are not symmetric, as is widely believed. The energy cost for building higher-mass quarks is much less than for antiquarks, and their ground states also differ. In particular, building an $\bar{s}$ antiquark from its ground state (i.e., $\bar{d} \to \bar{s}$) costs 182 more MeV than building an s quark from its own ground state, i.e., u → s (Figure A4). These charac-

teristic energy costs of (anti)quark transitions may be unobservable for now, but we hope they can at least be measured in lattice-QCD numerical simulations [50–53].

Author Contributions: D.M.C. and D.K. worked on all aspects of the problems. All authors have read and agreed to the published version of the manuscript.

Funding: This research received no external funding.

Data Availability Statement: The data analyzed in this work are publicly available from the Particle Data Group [1,2] and CODATA [3]. Baryon data are available in the review article of Thiel et al. [5]. New data generated from PDG data in the course of this study are listed in Tables 2–10 of this paper.

Acknowledgments: We thank the reviewers for comments and suggestions that helped us improve the presentation of the material.

Conflicts of Interest: The authors declare no conflicts of interest.

Abbreviations

The following abbreviations are used in this manuscript:

CODATA	Committee On Data
CP	Charge Parity
EM	Electromagnetic
LHCb	Large Hadron Collider beauty
NNG	Nakano–Nishijima–Gell-Mann
PDG	Particle Data Group
QCD	Quantum Chromodynamics
SM	Standard Model
ST	Strong

Appendix A. Mass Jumps between Particles

Figures A1–A3 illustrate the jumps in rest mass between individual particles in detail. All jumps are noted in MeV.

The corresponding average rest-mass energy levels are illustrated in Figures 4–6 in the main text, where the discrete jumps are more clearly seen between states for groups of related particles.

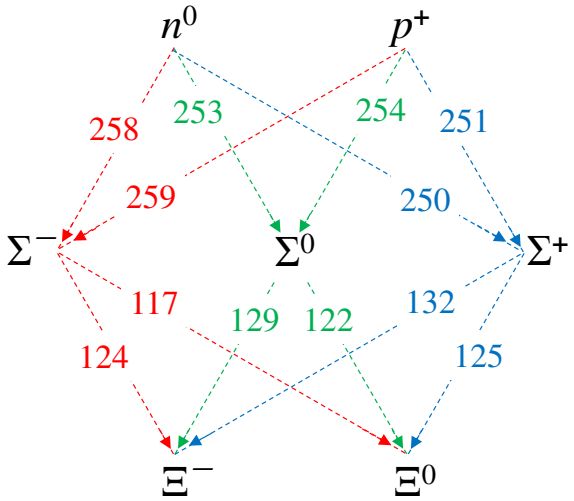

Figure A1. Detailed illustration of rest-mass energy levels for the $J^P = (1/2)^+$ baryons in Figure 4.

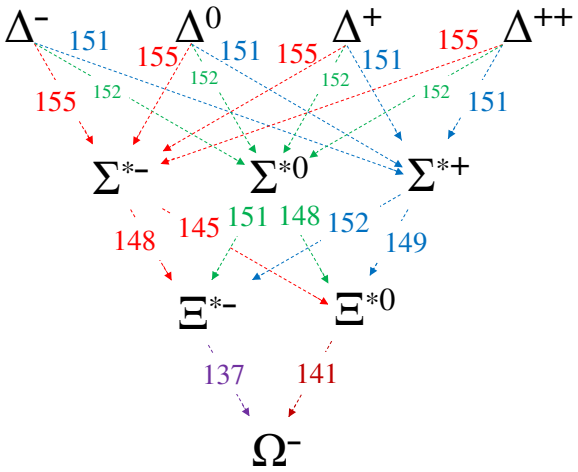

Figure A2. Detailed illustration of rest-mass energy levels for the $J^{\mathrm{P}} = (3/2)^{+}$ baryons in Figure 5.

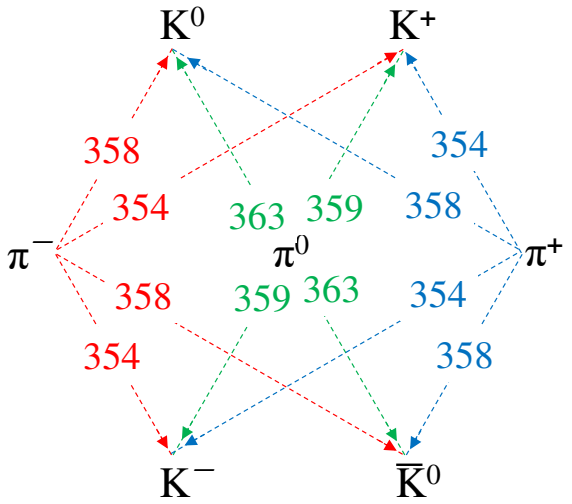

Figure A3. Detailed illustration of rest-mass energy levels for the low-mass $J^{\mathrm{P}} = 0^{-}$ pseudoscalar mesons in Figure 6.

Appendix B. Valence Quarks in Σ/Λ⁰/Ξ/Ω/Ξ* Baryons

Appendix B.1. Octet Σ *and* Λ^0 *Baryons*

The Σ^{+}(uus) baryon is unusual in the sense that it is less massive than the neutral Σ^{0}(uds), whereas Σ^{-}(dds) is the most massive particle in the Σ triplet (Table 2). It appears that the two low-mass u quarks in Σ^{+} are indirectly responsible for this unusual outcome, although it persists in the *MD*s after we also account for the repulsive Coulomb content of the $\Sigma^{\pm}$ particles. Σ^{+} has the same charge layout as the proton; thus, its strong field includes 1.22 MeV in suppressing the repulsion. Similarly, the strong field of Σ^{-} includes a Coulombic part of 1.00 MeV, as was found in Section 3.3). By subtracting the Coulombic contributions from the *MD*s of $\Sigma^{\pm}$ (Table 2), we obtain the remainders of the constituent energies (*ER*′) of the Σ excitations, viz.,

$$\left.\begin{array}{ll} \Sigma^{+}(\mathrm{uus}): & ER'_{\Sigma^{+}} = 1090.43 \\ \Sigma^{0}\,(\mathrm{uds}): & ER'_{\Sigma^{0}} = 1092.41 \\ \Sigma^{-}(\mathrm{dds}): & ER'_{\Sigma^{-}} = 1093.71 \end{array}\right\}\ \mathrm{MeV}. \tag{A1}$$

Dynamic strong-field support for two u quarks and one s quark is included in $ER'_{\Sigma^{+}}$, which is the lowest value. The other two higher values describe support for one and two d quarks relative to one and two u quarks, respectively, in $ER'_{\Sigma^{+}}$. But there is a caveat in

the case of Σ^0 that differentiates it from the charged members of the triplet, despite all members having isospin $I = 1$. Σ^0 is an excitation of Λ^0, which has $I = 0$, as opposed to $\Sigma^{\pm}$, which represents nucleonic ($I = 1/2$) excitations with isospin transitions of the form $I = 1/2 \to 1$. The cost in supporting the $I = 0 \to 1$ transition of $\Lambda^0 \to \Sigma^0$ can be obtained from the decay of $\Sigma^0 \to \Lambda^0 \gamma$, in which the emitted photon carries 76.959 MeV [1,2]. Thus, the $I = 0 \to 1$ cost in isospin energy (EI), rounded to two decimals, is

$$EI_{0\to 1} = 76.96 \text{ MeV}. \tag{A2}$$

It is important to note that hypercharge (Y) does not capture the above difference, as it changes uniformly ($Y = 1 \to 0$) in the nucleonic Λ and Σ excitations (Table 2).

Next, we consider transitions from the nucleonic ground state. We subtract the reference MD_{n} value of the neutron (n^0) from the ER' values listed in Equation (A1), and we find the building blocks of energy (ER) in the strong-field support of the $\Sigma^{\pm}$ and Λ^0 excitations, viz.,

$$\left.\begin{array}{lll} n^0 \to \Sigma^+ \ (\text{dd} \to \text{us}) & : & ER_{\Sigma^+} = 162.36 \\ n^0 \to \Sigma^- \ (\text{u} \to \text{s}) & : & ER_{\Sigma^-} = 165.64 \\ n^0 \to \Lambda^0 \ (\text{d} \to \text{s}) & : & ER_{\Lambda^0} = 87.38 \end{array}\right\} \text{MeV}. \tag{A3}$$

These energy values include the energy to maintain the newborn valence quarks (e.g., quarks u, s in Σ^+ relative to quarks d, d in n^0), and the energy costs for the limpid changes in isospin energy between states ($EI_{1/2\to 1}$ for $\Sigma^{\pm}$ and $EI_{1/2\to 0}$ for Λ^0).

The above energy costs introduce more unknowns than the experimental data can handle. Then, it is common practice in physics to adopt a physical model capable of resolving the indeterminacy. In what follows, we incorporate several additional (yet physically reasonable) assumptions concerning the various energy differences between states.

(1a) The energy cost to maintain a quark flip becomes a gain when the quarks flip in the opposite direction, that is, the energies of the u→d and d→u quark flips obey $E_{\text{u}\to\text{d}} = -E_{\text{d}\to\text{u}}$ and so on for all the other flips. Thus, quark flipping is assumed to be a reversible process.

(1b) The same property also holds for isospin transition energies, viz., $EI_{1/2\to 0} = -EI_{0\to 1/2}$ and $EI_{1/2\to 1} = -EI_{1\to 1/2}$. Thus, an isospin transition is assumed to be a reversible process as well.

(2a) The energy cost to maintain a u→s quark flip is the sum of the costs of the u→d and d→s flips, that is, the energies obey $E_{\text{u}\to\text{s}} = E_{\text{u}\to\text{d}} + E_{\text{d}\to\text{s}}$ and so on for all the other striding quark flips.

(2b) The same property also holds for the isospin transition energies, that is, $EI_{0\to 1} = EI_{0\to 1/2} + EI_{1/2\to 1}$.

Based on the above considerations, we use the values listed in Equation (A3) to set up a 3×4 system of equations describing the breakdown of the various excitation energies relative to the n^0 nucleonic ground state, viz.,

$$\left.\begin{array}{rcl} -E_{\text{u}\to\text{d}} + E_{\text{d}\to\text{s}} + EI_{1/2\to 1} & = & 162.36 \\ E_{\text{u}\to\text{d}} + E_{\text{d}\to\text{s}} + EI_{1/2\to 1} & = & 165.64 \\ E_{\text{d}\to\text{s}} - EI_{0\to 1/2} & = & 87.38 \end{array}\right\} \text{MeV}. \tag{A4}$$

The solution of this system specifies a unique value of

$$E_{\text{u}\to\text{d}} = 1.64 \text{ MeV}, \tag{A5}$$

and the reduced 2×3 system is

$$\left.\begin{array}{rcl} EI_{1/2\to 1} + E_{\text{d}\to\text{s}} & = & 164.00 \\ EI_{1/2\to 1} + EI_{0\to 1/2} & = & 76.62 \end{array}\right\} \text{MeV}. \tag{A6}$$

The latter equation *appears* to justify assumption (4) above; it implies that $EI_{0\to1} = 76.62$ MeV, which is barely 0.44% lower than the measured value quoted in Equation (A2).

However, we do not believe that this small discrepancy of 0.34 MeV is due to the many approximations and assumptions incorporated in our calculations, and it is certainly not due to the many experimental values that we used above. Instead, we think that the 0.34 MeV difference indicates a missing energy term (EI_0) that represents the initial cost of switching states from $I = 0$ to $I = 0 + \varepsilon$, where $\varepsilon \to 0$ (i.e., the energy associated with the birth of the isospin property in strong interactions).

If we further assume that

$$EI_{0+\varepsilon\to1/2} = EI_{1/2\to1}\,,$$

in actual $I \neq 0$ isospin transitions, we obtain a complete solution and a clear picture of light-quark transitions in low-energy octet baryons, viz.,

$$\left.\begin{array}{lcr} E_{\mathrm{u}\to\mathrm{d}} & = & 1.64 \\ E_{\mathrm{d}\to\mathrm{s}} & = & 125.69 \\ E_{\mathrm{u}\to\mathrm{s}} & = & 127.33 \\ EI_{\delta I=+\frac{1}{2}} & = & 38.31 \\ EI_{\delta I=+1} & = & 76.62 \\ EI_0 & = & 0.34 \end{array}\right\} \text{MeV}, \tag{A7}$$

where $EI_{\delta I} > 0$ is the associated energy cost during transitions between states (obeying the property that $EI_{-\delta I} = -EI_{\delta I}$), and $EI_0 > 0$ is the energy cost to jump-start a transition from an initial $I = 0$ state, viz.,

$$EI_0 + EI_{\delta I=+1} = 76.96 \text{ MeV} \;\equiv\; EI_{0\to1}\,, \tag{A8}$$

as in the fundamental experimental result described by Equation (A2) above. Furthermore,

$$EI_0 + EI_{\delta I=+1/2} = 38.65 \text{ MeV} \;\equiv\; EI_{0\to1/2}\,, \tag{A9}$$

for the complete half-way process ($EI_{0\to1/2}$) with isospin change of $I \equiv 0 \to 1/2$.

Appendix B.2. Discussion of the Σ-Λ^0 *Results*

There is a wealth of information in the above results. Here, we highlight a few key points.

(a) The u→d quark flip is inexpensive ($E_{\mathrm{u}\to\mathrm{d}} = 1.64$ MeV). This explains why u→d is the only flip to a higher-mass quark in the quark sequence [38]. The transition involves the exchange of a virtual W^- boson with a mass of 80.377 GeV [2], so the actual flipping cost ($E_{\mathrm{u}\to\mathrm{d}}$) is truly negligible. Also, there is no energy charge for $I_3 = \pm1/2 \to \mp1/2$ changes in u←→d flips, as we already know from the p^+-n^0 results of Section 3.1. Furthermore, the small energy budget involved in u←→d flips is consistent with the ubiquity of the $\beta^\pm$ decays via weak interactions [38,54].

(b) The decays of s→u and s→d release substantial amounts of energy (126–127 MeV). This energy is ∼64% larger than the isospin transition energy of 76.96 MeV quoted in Equation (A8) above—comparable to the differences in rest mass between Σ and Ξ baryons (Figure 4) to the rest masses (Table 4) of the pions emitted in $\Xi \to \Lambda^0\,\pi$ decays (Table 6).

(c) The energy release from $\delta I = -1/2$ changes is small (e.g., $EI_{1/2\to0} = -38.65$ MeV, about 30% of $E_{\mathrm{u}\to\mathrm{s}}$), but this energy also becomes available to the surrounding strong field for other tasks.

(d) A curious finding is the following: We define by $E > 0$ the energy needed to support a quark flip to a higher-mass s quark (i.e., d→s or u→s, as in Equation (A7)), plus

the 1-MeV anti-Coulombic contribution of u→s in $n^0 \rightarrow \Sigma^-$ (Section 3.3); and by $\delta m > 0$ the rest-energy differential between the two quarks; then, we find that the corresponding "mass deficit" is effectively the same in both cases, viz.

$$MD_{\mathrm{u,d}\rightarrow\mathrm{s}} \equiv (E - \delta m)_{\mathrm{u,d}\rightarrow\mathrm{s}} = 37\ \mathrm{MeV}; \tag{A10}$$

as it should be, since EM forces and quark rest-mass differences have been accounted for, and the isospin energy ($EI_{1/2\rightarrow 0}$) is the same in both cases ($I_3 = 0$ for the s quark; Table 5).

(e) Despite the similarity between cases in item (d), the decay of s→u dominates entirely in nature (s→d, in which $Q = -1/3 \rightarrow -1/3$ does not occur), but for an EM-related reason. Virtual neutral-vector bosons (Z^0) do not mediate quark transitions [6,38], and $W^{\pm}$ bosons always modify the quark charge. This prevents weak s→d transitions and makes the EM charge factor of $\vartheta_{\mathrm{e}} = 2$ (Section 2.2 and Table 5) all the more important for the quarks that own it (residing in u- and c-flavored hadrons).

Appendix B.3. Octet Ξ Baryons

The Ξ baryons contain two s quarks, in contrast to Λ^0 (one s quark), and they undergo only $\Xi \rightarrow \Lambda^0\,\pi$ decays (Table 6). We analyzed the energy budget of the transitions of $\Lambda^0 \rightarrow \Xi$ in the same way and with the same assumptions as above, and we obtained the transition energies necessary to support the appearance of the second s quark in Ξ baryons. By doing so, we shifted our analysis into the second highest energy level of excited states in the $J^{\mathrm{P}} = (1/2)^+$ baryon octet; these states are effectively defined by the birth of a second s quark from first-generation quarks. The same results can be obtained by considering the transitions of $n^0 \rightarrow \Xi$, in which two s quarks are born together and the isospin ($I = 1/2$) does not change and does not play a role.

Here, we summarize the energy budget of the various processes responsible for the appearance of the second s quark ($\Lambda^0 \rightarrow \Xi^0$, where $\mathrm{d}\rightarrow\mathrm{s}^{(2)}$, and $\Lambda^0 \rightarrow \Xi^-$, where $\mathrm{u}\rightarrow\mathrm{s}^{(2)}$). The isospin changes from $I = 0$ to $I = 1/2$ in both cases. The energy remainders $ER^{(2)}$ in the strong-field support of the $\Lambda^0 \rightarrow \Xi$ excitations are

$$\left.\begin{array}{lll} \Lambda^0 \rightarrow \Xi^0 \ \ (\mathrm{d}\rightarrow\mathrm{s}): & ER^{(2)}_{\Xi^0} = 110.45 \\ \Lambda^0 \rightarrow \Xi^- \ \ (\mathrm{u}\rightarrow\mathrm{s}): & ER^{(2)}_{\Xi^-} = 113.79 \end{array}\right\} \mathrm{MeV}, \tag{A11}$$

where the anti-Coulombic contribution of 1.00 MeV is subtracted from $ER^{(2)}_{\Xi^-}$. The corresponding system of equations for the energy components of quark transitions takes the form of

$$\left.\begin{array}{lll} E^{(2)}_{\mathrm{d}\rightarrow\mathrm{s}} + EI_{0\rightarrow 1/2} &=& 110.45 \\ E^{(2)}_{\mathrm{u}\rightarrow\mathrm{s}} + EI_{0\rightarrow 1/2} &=& 113.79 \end{array}\right\} \mathrm{MeV}, \tag{A12}$$

where $EI_{0\rightarrow 1/2}$ is given by Equation (A9). The solution of this system is

$$\left.\begin{array}{lll} E^{(2)}_{\mathrm{d}\rightarrow\mathrm{s}} &=& 71.80 \\ E^{(2)}_{\mathrm{u}\rightarrow\mathrm{s}} &=& 75.14 \end{array}\right\} \mathrm{MeV}. \tag{A13}$$

Subtracting these two values, we find that $E^{(2)}_{\mathrm{u}\rightarrow\mathrm{d}} = 3.34$ MeV; thus, when the second s quark appears, the cost for also flipping the remaining quark (u→d) effectively doubles (hypothetically, since $\Xi^- \rightarrow \Xi^0$ does not occur).

Combining the quark transition energies from Equations (A7) and (A13) and rounding off to one decimal for convenience, we determine that

$$\left.\begin{array}{rcl} E_{\mathrm{uu}\to\mathrm{ss}} & = & 202.5 \\ E_{\mathrm{ud}\to\mathrm{ss}} & = & 200.0 \\ E_{\mathrm{dd}\to\mathrm{ss}} & = & 197.5 \end{array}\right\} \text{MeV}. \tag{A14}$$

Here, the 2.5 MeV differences mimic differences in u and d quark rest masses ($m_{\mathrm{d}} - m_{\mathrm{u}} = 2.5$ MeV; Table 5), but they do not stem from quark rest masses, which were taken out of the *MD*s that gave us Equation (A11). Instead, they reflect the following property of the two light quarks flipping to s quarks.

We use the binding energies in Equation (A14) to derive the "mass deficits" of two-quark s transitions (as in Equation (A10) above for one-quark s transitions), viz.,

$$MD_{\mathrm{qq'}\to\mathrm{ss}} \equiv (E - \delta m)_{\mathrm{qq'}\to\mathrm{ss}} = 20 \text{ MeV}, \tag{A15}$$

where qq′ represents any of the pairs (uu, dd, or ud).

Appendix B.4. The Ω^- Baryon

Although not a member of the baryon octet, Ω^- is of special interest, as it contains three s quarks. Its decays $\Omega^- \to \Xi\,\pi$ and $\Omega^- \to \Lambda^0\,\mathrm{K}^-$ also involve a change of spin of $J = 3/2 \to 1/2$, whereas parity is conserved [1,2,38,39]. At the same time, the $J = 3/2$ Ξ^* baryons also decay to $J = 1/2$ Ξ baryons ($\Xi^* \to \Xi\,\pi$). Thus, we have an opportunity to study the energy requirement ($E^{(3)}_{\mathrm{u,d}\to\mathrm{s}}$) for a third s quark to appear in the transition of $\Xi^* \to \Omega^-$ and to determine the energy ($EJ_{\delta J=-1}$) released due to spin change in the transitions of $\Xi^* \to \Xi$, in which isospin $I = 1/2$ and $\delta I = 0$ (see Appendix B.5 below).

Using the above methodology and assumptions, for $\Xi^* \to \Omega^-$, we find that

$$\left.\begin{array}{rcl} E^{(3)}_{\mathrm{d}\to\mathrm{s}} & = & 87.37 \\ E^{(3)}_{\mathrm{u}\to\mathrm{s}} & = & 87.06 \end{array}\right\} \text{MeV}, \tag{A16}$$

a somewhat surprising result ($E^{(3)}_{\mathrm{d}\to\mathrm{s}} \approx E^{(3)}_{\mathrm{u}\to\mathrm{s}}$) that may yet be valid at the high energies considered here. Furthermore, by combining Equations (A14) and (A16), we find that

$$\left.\begin{array}{rcl} E_{\mathrm{uuu}\to\mathrm{sss}} & \simeq & 290 \\ E_{\mathrm{ddd}\to\mathrm{sss}} & \simeq & 285 \end{array}\right\} \text{MeV}. \tag{A17}$$

We reiterate that the transition of s→d does not occur in nature [6,38], so the 285 MeV cost determined here is of theoretical interest only.

Appendix B.5. Ξ^* Baryon Decays Emitting Pions

The Ξ^* baryons invariably decay to Ξ baryons, emitting a pion ($\Xi^* \to \Xi\,\pi$; Tables 7 and 10) [1,2]. The energy released in these four reactions comes from the change in spin in the transitions of $\Xi^* \to \Xi$, viz.,

$$\delta J = -1\,, \tag{A18}$$

where no spin energy is stored in the $J = 0$ pion (isospin energy is included in the rest masses of the fragments). This allows for a determination of the kinetic energy (KE_π) imparted to the pion in each of these decays.

From energy conservation in the $\Xi^* \to \Xi\,\pi$ decays, we find that

$$KE_\pi = 77.8^{+4.1}_{-7.3} \text{ MeV}. \tag{A19}$$

This average value compares well to the 77 MeV of energy released in the decay of $\Sigma^0 \rightarrow \Lambda^0 \gamma$ due to the change in isospin ($\delta I = -1$). Thus, this is another instance where isospin behaves quantitatively like spin (which was the basis for Heisenberg's original design of the isospin vector [55]).

The error bar in KE_π indicates missing physics in intermediate steps (weak interactions), mostly in the decays of Ξ^{*0} that resulted in the largest deviations from the mean. The decay of $\Xi^{*0} \rightarrow \Xi^- \pi^+ (+70.5 \text{ MeV})$ is particularly noted because charges appear "out of nowhere" and the cost of "jump-starting" the charge in the initial neutral state is unknown.

Because pions are also emitted in kaon decays, we can obtain independent estimates of their shared kinetic energy. In particular, kaons exhibit a set of hadronic modes (most with significant frequencies of occurrence (Γ_i/Γ), the so-called *branching ratios*), some of which produce three pions [1,2,38], viz.,

$$\left.\begin{array}{ll} K^\pm \rightarrow \pi^+ \pi^- \pi^\pm, & \Gamma_{11}/\Gamma = 5.583\,\% \\ K^0_{(L)} \rightarrow \pi^+ \pi^- \pi^0, & \Gamma_7/\Gamma = 12.54\,\% \end{array}\right\}. \tag{A20}$$

From energy conservation in these reactions, we find that the average total kinetic energy imparted to the three pions is

$$KE_{3\pi} = 77.8^{+5.7}_{-2.8} \text{ MeV}. \tag{A21}$$

The error bar here is about 3 MeV shorter than that in Equation (A19). Accordingly, an energy release of about 77 MeV is common in hadron decays in which pions or photons are emitted.

The $KE_{3\pi}$ value in Equation (A21) is the smallest amount of total kinetic energy that can be produced in nonet hadronic modes because nonet kaons do not have enough energy to decay to four pions. For comparison purposes, the ω vector meson that can decay to four pions ($\omega \rightarrow 2\pi^+ 2\pi^-$, $\Gamma_{12}/\Gamma < 0.1\,\%$) imparts a total of $KE_{4\pi} = 224$ MeV ($\sim$3 times as much) to the pions.

Appendix C. Valence Antiquarks in K and π Pseudoscalar Mesons

Nonet $J^P = 0^-$ kaons decay to pions with an isospin change per pion of

$$\delta I = +1/2\,, \tag{A22}$$

and no spin-parity (CP) change occurs across the reactions ($\delta J^{\delta P} = 0^0$). An examination of (anti)quark flipping in $K \rightarrow \pi$ transitions allows us to investigate the energy budget of antiquarks. The results are not simply a dry overview of those obtained for quarks in Appendix B. As we will see, the antiquarks have different transition energies ($E_{\bar{q}\rightarrow\bar{q}'}$) and different energy levels, in which $\bar{d}$ appears to be the actual ground state.

Again using the methodology and the assumptions described in Appendix B, for $\pi^0 \rightarrow K^0$ (where π^0 is approximately the mixed state $((|u\bar{u}\rangle - |d\bar{d}\rangle)/\sqrt{2})$), we find that the remaining energy is

$$\left.\begin{array}{ll} \pi^0 \rightarrow K^0 \ (u\bar{u} \rightarrow d\bar{s}) : & ER_{u\bar{u}} = 271.39 \text{ MeV} \\ \pi^0 \rightarrow K^0 \ (d\bar{d} \rightarrow d\bar{s}) : & ER_{d\bar{d}} = 271.39 \text{ MeV} \end{array}\right\}. \tag{A23}$$

The value of ER in charged transitions ($\pi^\pm \rightarrow K^\pm$) is 6.02 MeV smaller, and it is not used in the calculations that follow. The origin of the difference is purely electromagnetic; this value is the sum of the 4.59 MeV difference in pions and the 1.43 MeV difference in kaons (MD values are listed in Table 4).

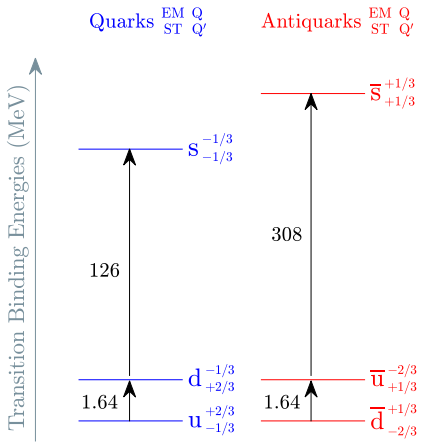

Figure A4. Quark and antiquark transition energies for the three lower-energy states in each group. The diagram is drawn on a logarithmic scale. Binding-energy jumps are quoted to three significant digits. The binding energy of $\bar{u} \to \bar{s}$ is 2.4 times larger than that of the u→s transition, pointing to the origin of CP violation.

Using the (anti)quark transitions of Equation (A23), we derive the following system of equations:

$$\left.\begin{array}{rcl} E_{u\to d} + E_{\bar{u}\to\bar{s}} + EI_{1\to 1/2} &=& 271.39 \\ E_{\bar{d}\to\bar{s}} + EI_{1\to 1/2} &=& 271.39 \end{array}\right\} \text{MeV}, \tag{A24}$$

where $E_{u\to d} = 1.64$ MeV and $EI_{1\to 1/2} = -38.31$ MeV (Appendix B). The solution of system (A24) is

$$\left.\begin{array}{rcl} E_{\bar{u}\to\bar{s}} &=& 308.06 \\ E_{\bar{d}\to\bar{s}} &=& 309.70 \end{array}\right\} \text{MeV}, \tag{A25}$$

from which we obtain, by subtraction, the following astonishing result:

$$E_{\bar{u}\to\bar{d}} = -1.64 \text{ MeV}, \tag{A26}$$

that is, the antiquark transition of $\bar{u} \to \bar{d}$ releases energy back to the strong field. This implies that $\bar{d}$ is the actual antiquark ground state, and it lies below $\bar{u}$ by the same amount of binding energy (1.64 MeV) as the u-quark ground state lies below the d quark.

Precisely the same results were also obtained by two alternative calculations, namely (a) by considering the equations for the alternative (anti)quark paths ($(u \to \bar{s}, \bar{u} \to d)$ and $(d \to \bar{s}, \bar{d} \to d)$) and (b) by considering the path of $\frac{1}{2}\left(u\bar{u} + d\bar{d}\right) \to K^0$. These results imply that the systems of equations that we solve on these paths are self-consistent; at the same time, the equations imply that there is no preferred path in (anti)quark flips during $\pi^0 \to K^0$ transitions, since all paths are energetically equivalent.

The energy budgets for quark and antiquark transitions are illustrated in Figure A4, assuming that the two ground states lie at the same energy level. It appears that strong-field support of the $\bar{s}$ antiquark in a bound state is about 2.4 times more expensive than that of the s quark, and this is grounds for the emergence of CP violation (see also item (4b) in Section 6.2 of the main text).

References

1. Zyla, P.A.; Barnett, R.M.; Beringer, J.; Dahl, O.; Dwyer, A.D.; Groom, E.D.; Lin, C.J.; Lugovsky, K.S.; Pianori, E.; Robinson, J.D.; et al. Review of Particle Physics (RPP 2020). *Prog. Theor. Exp. Phys.* **2020**, *2020*, 083C01.
2. Particle Data Group; Workman, R.L.; Burkert, V.D.; Crede, V.; Klempt, E.; Thoma, U.; Tiator, L.; Agashe, K.; Aielli, G.; Allanach, B.C.; et al. 2022 Review of particle physics. *Prog. Theor. Exp. Phys.* **2022**, *2022*, 083C01.
3. Tiesinga, E.; Mohr, P.J.; Newell, D.B.; Taylor, B.N. CODATA recommended values of the fundamental physical constants: 2018. *Rev. Mod. Phys.* **2021**, *93*, 025010. [CrossRef]
4. Frisch, D.H.; Thorndike, A.M. *Elementary Particles*; Van Nostrand: New York, NY, USA, 1964.

5. Thiel, A.; Afzal, F.; Wunderlich, Y. Light baryon spectroscopy. *Prog. Part. Nucl. Phys.* **2022**, *125*, 103949.
6. Peskin, M.E.; Schroeder, D.V. *An Introduction to Quantum Field Theory*; CRC Press: Boca Raton, FL, USA, 1995.
7. Bali, G.S. QCD forces and heavy quark bound states. *Phys. Rep.* **2001**, *343*, 1. [CrossRef]
8. Durr, S.; Fodor, Z.; Frison, J.; Hoelbling, C.; Hoffmann, R.; Katz, S.D.; Krieg, S.; Kurth, T.; Lellouch, L.; Lippert, T.; et al. Ab initio determination of light hadron masses. *Science* **2008**, *322*, 1224. [CrossRef] [PubMed]
9. Yang, Y.B.; Liang, J.; Bi, Y.J.; Chen, Y.; Draper, T.; Liu, K.F.; Liu, Z. Proton mass decomposition from the QCD energy momentum tensor. *Phys. Rev. Lett.* **2018**, *121*, 212001. [CrossRef]
10. Metz, A.; Pasquini, B.; Rodini, S. Understanding the proton mass in QCD. *SciPost Phys. Proc.* **2022**, *8*, 105. [CrossRef]
11. Pohl, R.; Antognini, A.; Nez, F.; Amaro, F.D.; Biraben, F.; Cardoso, J.M.; Covita, D.S.; Dax, A.; Dhawan, S.; Fernandes, L.M.; et al. The size of the proton. *Nature* **2010**, *466*, 213. [CrossRef] [PubMed]
12. Antognini, A.; Nez, F.; Schuhmann, K.; Amaro, F.D.; Biraben, F.; Cardoso, J.M.; Covita, D.S.; Dax, A.; Dhawan, S.; Diepold, M.; et al. Proton Structure from the Measurement of 2S-2P Transition Frequencies of Muonic Hydrogen. *Science* **2013**, *339*, 417. [CrossRef]
13. Bezginov, N.; Valdez, T.; Horbatsch, M.; Marsman, A.; Vutha, A.C.; Hessels, E.A. A measurement of the atomic hydrogen Lamb shift and the proton charge radius. *Science* **2019**, *365*, 1007. [CrossRef]
14. Xiong, W.; Gasparian, A.; Gao, H.; Dutta, D.; Khandaker, M.; Liyanage, N.; Pasyuk, E.; Peng, C.; Bai, X.; Ye, L.; et al. A small proton charge radius from an electron–proton scattering experiment. *Nature* **2019**, *575*, 147. [CrossRef] [PubMed]
15. Karr, J.P.; Marchand, D.; Voutier, E. The proton size. *Nat. Rev. Phys.* **2020**, *2*, 601. [CrossRef]
16. Ericson, T.; Weise, W. *Pions and Nuclei*; Oxford University Press: New York, NY, USA, 1988.
17. Borsanyi, S.; Durr, S.; Fodor, Z.; Hoelbling, C.; Katz, S.D.; Krieg, S.; Lellouch, L.; Lippert, T.; Portelli, A.; Szabo, K.K.; et al. Ab initio calculation of the neutron-proton mass difference. *Science* **2015**, *347*, 1452. [CrossRef] [PubMed]
18. Gasser, J.; Leutwyler, H. Implications of scaling for the proton-neutron mass difference. *Nucl. Phys. B* **1975**, *94*, 269. [CrossRef]
19. Thomas, A.W.; Wang, X.G.; Young, R.D. Electromagnetic contribution to the proton-neutron mass splitting. *Phys. Rev. C* **2015**, *91*, 015209. [CrossRef]
20. Erben, F.B.; Shanahan, P.E.; Thomas, A.W.; Young, R.D. Dispersive estimate of the electromagnetic charge symmetry violation in the octet baryon masses. *Phys. Rev. C* **2014**, *90*, 065205. [CrossRef]
21. Gasser, J.; Hoferichter, M.; Leutwyler, H.; Rusetsky, A. Cottingham formula and nucleon polarizabilities. *Eur. Phys. J. C* **2015**, *75*, 375. [CrossRef]
22. Gasser, J.; Leutwyler, H.; Rusetsky, A. Sum rule for the Compton amplitude and implications for the proton–neutron mass difference. *Eur. Phys. J. C* **2020**, *80*, 1121. [CrossRef]
23. Gasser, J.; Leutwyler, H.; Rusetsky, A. On the mass difference between proton and neutron. *Phys. Lett. B* **2021**, *814*, 136087. [CrossRef]
24. Leutwyler, H. Theoretical aspects of chiral dynamics. In Proceedings of the 8th International Workshop on Chiral Dynamics—PoS(CD15), Pisa, Italy, 29 June–3 July 2015.
25. Walker-Loud, A.; Carlson, C.E.; Miller, G.A. Electromagnetic self-energy contribution to $M_p - M_n$ and the isovector nucleon magnetic polarizability. *Phys. Rev. Lett.* **2012**, *108*, 232301. [CrossRef] [PubMed]
26. Sato, K.; Watanabe, H.; Yamazaki, T. Calculation of the pion charge radius from an improved model-independent method. In Proceedings of the 39th International Symposium on Lattice Field Theory—PoS(LATTICE2022), Bonn, Germany, 8–13 August 2022.
27. Duran, B.; Meziani, Z.E.; Joosten, S.; Jones, M.K.; Prasad, S.; Peng, C.; Armstrong, W.; Atac, H.; Chudakov, E.; Bhatt, H.; et al. Determining the gluonic gravitational form factors of the proton. *Nature* **2023**, *615*, 813. [CrossRef] [PubMed]
28. Bars, I.; Hanson, A.J. Quarks at the ends of the string. *Phys. Rev. D* **1976**, *13*, 1744. [CrossRef]
29. Kalashnikova, Y.S.; Nefediev, A.V. 1 + 1 string with quarks at the ends revisited. *Phys. Lett. B* **1997**, *399*, 274. [CrossRef]
30. Nefediev, A.V. Light-light and heavy-light mesons in the model of QCD string with quarks at the ends. *AIP Conf. Proc.* **2002**, *619*, 595.
31. Pasechnik, R.; Šumbera, M. Phenomenological review on quark-gluon plasma: Concepts vs. observations. *Universe* **2017**, *3*, 7. [CrossRef]
32. Fritzsch, H. Quarks. In *Murray Gell-Mann and the Physics of Quarks*; Birkhäuser: Cham, Switzerland, 2018.
33. Bulava, J.; Hörz, B.; Knechtli, F.; Koch, V.; Moir, G.; Morningstar, C.; Peardon, M. String breaking by light and strange quarks. *Phys. Lett. B* **2019**, *793*, 493. [CrossRef]
34. Coleman, S.; Glashow, S.L. Electrodynamic properties of baryons in the unitary symmetry scheme. *Phys. Rev. Lett.* **1961**, *6*, 423. [CrossRef]
35. Nakano, T.; Nishijima, K. Charge independence for V-particles. *Prog. Theor. Phys.* **1953**, *10*, 581. [CrossRef]
36. Nishijima, K. Charge independence theory of V particles. *Prog. Theor. Phys.* **1955**, *13*, 285. [CrossRef]
37. Gell-Mann, M. The interpretation of the new particles as displaced charge multiplets. *Nuovo C.* **1956**, *4* (Suppl. S2), 848. [CrossRef]
38. Rohlf, J.W. *Modern Physics*; John Wiley: New York, NY, USA, 1994.
39. Barnes, V.E.; Connolly, P.L.; Crennell, D.J.; Culwick, B.B.; Delaney, W.C.; Fowler, W.B.; Hagerty, P.E.; Hart, E.L.; Horwitz, N.; Hough, P.V.C.; et al. Observation of a hyperon with strangeness minus three. *Phys. Rev. Lett.* **1964**, *12*, 204. [CrossRef]
40. Povh, B.; Rith, K.; Scholz, C.; Zetsche, F.; Rodejohann, W. *Particles and Nuclei*, 4th ed.; Springer: Berlin, Germany, 2004.

41. Christman, J.R. *Isospin: Conserved in Strong Interactions*. 2001. Available online: www.physnet.org/modules/pdf_modules/m278.pdf (accessed on 26 October 2023).
42. Miller, A.I. *137: Jung, Pauli, and the Pursuit of a Scientific Obsession*; WW Norton: New York, NY, USA, 2009.
43. Eichten, E.; Gottfried, K.; Kinoshita, T.; Lane, K.D.; Yan, T.M. Charmonium: The model. *Phys. Rev. D* **1978**, *17*, 3090. [CrossRef]
44. Dimopoulos, S.; Susskind, L. Baryon number of the universe. *Phys. Rev. D* **1978**, *18*, 4500. [CrossRef]
45. Shaposhnikov, M.E.; Farrar, G.R. Baryon asymmetry of the universe in the Minimal Standard Model. *Phys. Rev. Lett.* **1993**, *70*, 2833.
46. Riotto, A.; Trodden, M. Recent progress in baryogenesis. *Ann. Rev. Nucl. Part Sci.* **1999**, *49*, 46. [CrossRef]
47. Canetti, L.; Drewes, M.; Shaposhnikov, M. Matter and antimatter in the universe. *New J. Phys.* **2012**, *14*, 095012. [CrossRef]
48. The LHCb Collaboration. Measurement of matter-antimatter differences in beauty baryon decays. *Nat. Phys.* **2017**, *13*, 391. [CrossRef]
49. The LHCb Collaboration. Observation of CP violation in charm decays. *Phys. Rev. Lett.* **2019**, *122*, 211803. [CrossRef]
50. Davies, C.T.; Follana, E.; Gray, A.; Lepage, G.P.; Mason, Q.; Nobes, M.; Shigemitsu, J.; Trottier, F.H.; Wingate, M.; Aubin, C. High-precision lattice QCD confronts experiment. *Phys. Rev. Lett.* **2004**, *92*, 022001. [CrossRef]
51. De Grand, T.; De Tar, C. *Lattice Methods for Quantum Chromodynamics*; World Scientific: Singapore, 2006.
52. Gattringer, C.; Lang, C.B. *Quantum Chromodynamics on the Lattice*; Springer: Berlin, Germany, 2010.
53. Bazanov, A. Nonperturbative QCD simulations with 2 + 1 flavors of improved staggered quarks. *Rev. Mod. Phys.* **2010**, *82*, 1349. [CrossRef]
54. Kónya, J.; Nagy, N.M. *Nuclear and Radiochemistry*, 2nd ed.; Elsevier: Amsterdam, The Netherlands, 2018.
55. Heisenberg, W. Über den Bau der Atomkerne. I. *Z. Phys.* **1932**, *77*, 1. [CrossRef]